Thesis Proposal

Space Environment Impacts on Geostationary Communications Satellites

---

Whitney Quinne Lohmeyer
Ph.D Candidate

Massachusetts Institute of Technology
Department of Aeronautics & Astronautics
Space Systems Lab

Submitted on: April 22, 2013

Thesis Committee: Kerri Cahoy, Daniel Hastings, and Yuri Shprits

Table of Contents

Abstract

Energetic particles in our space environment can damage geostationary communications satellite systems. However, it is difficult to obtain satellite telemetry, which is required to accurately understand the causal relationship of space weather and satellite performance and to quantify the actual effects of the space environment on these satellites. We approach this challenge by teaming with two communications satellite operators, Inmarsat and Telenor, to acquire telemetry data. We analyze more than one million operational hours (~7 GB) of telemetry and anomaly data. Our goals are to 1) capture the future capabilities and designs for geostationary communications satellites, focusing on the advancing capabilities of power amplifiers, 2) characterize the relationship of the space weather environment, in terms of low-energy electrons, the Kp index, high-energy protons and electrons, and galactic cosmic rays, with the performance of geostationary communication satellites, and 3) determine if geostationary communication satellite telemetry can be used to infer observations of the space environment. Our approach to addressing these research goals is to first analyze the telemetry from two different types of power amplifiers on the Inmarsat and Telenor satellites and to summarize the hardware susceptibility to anomalies. This analysis will extend three prior studies conducted in 1991, 1993, and 2005 that compare two amplifier technologies: solid-state power amplifiers (SSPAs), which are onboard the Inmarsat satellites, and traveling wave tube amplifiers (TWTAs), which are onboard the Telenor satellites. We will also obtain space environment data from the OMNI2 database, the Geostationary Operational Environmental Satellite (GOES), the Solar Influences Data Center, and Los Alamos National Labs (LANL) geostationary satellites. We will compare this data with the Inmarsat and Telenor telemetry to statistically understand the space environment at the time of anomalies, and for periods of two weeks prior to each of the satellite anomalies. Additionally we will design an algorithm that examines all satellite telemetry, not just at the time of known anomalies, and determine if satellite telemetry can accurately relay information on space environment activity and the satellite system itself. This work will uniquely incorporate geostationary satellite telemetry to better understand the effects of space weather on satellite systems to improve satellite performance as well as current and future satellite design.

1. Problem Statement and Objectives

In 2008, the National Research Council published the "Severe Space Weather Events – Understanding Societal and Economic Impacts Workshop Report". This report documents the findings from the 2007 public workshop that the Space Studies Board (SSB) of the National Academies was charged to convene to assess the nation's ability to manage the effect of space weather and their societal and economic impacts [*NRC*, 2008].

One of the primary technologies of focus was the telecommunications satellite industry. At the time of the workshop more than 250 geostationary communications satellites were in orbit, which amounted to more than a $75 billion dollar investment that delivered an annual revenue of $25 billion. Economics aside, this critical infrastructure of these satellites is important because of the services it provides. To name a few, these satellites provide backup communication in the event of a disaster that damages ground based communications systems, they provide news, education, and entertainment to remote areas, and connect end users including military, maritime officials, or civilian subscribers.

1.1 Problem Statement

The telecommunications industry has to manage the effects of space weather, which not only affects the geostationary communication satellite hardware, but also the satellite engineers, satellite operators, and satellite customers. For example, in 1994, Canadian Telesat experienced a space weather induced satellite anomaly when their Anik E2 satellite went off air due to an energetic electron induced discharge to the momentum wheel control circuitry [*Shea et al.,* 1998]. As a result, more than 100,000 dish owners and 1,600 remote communities were affected. Fortunately, the $290 million dollar satellite was restored after an intensive six month, $70 million recovery effort [*Gubby et al.,* 2002]. Numerous other examples of space weather induced anomalies exist, yet the primary challenge lies in understanding how to quantify the effects of space weather on satellite components [*NRC,* 2008]. Electrical upsets, hardware anomalies, interference, and solar array degradation are just a few of the known effects of the space environment [*Koons et al.,* 2000; *Gubby et al.,* 2002]. As a result of space weather, satellite operators are occasionally forced to manage satellites with reduced capabilities or fully decommission satellites, amounting to social and economic losses of several tens of millions of dollars per year [*Baker*, 1998; *Wilkinson,* 2000; *Barbieri et al.,* 2004].

One of the 2008 NRC Workshop - "Severe Space Weather Events – Understanding Societal and Economic Impacts Workshop" conclusions was that access to space weather data as well as satellite telemetry is the first step in better understanding to what extent space weather is related to the cause of satellite anomalies. While it is widely known that space weather impacts the performance of satellite systems [e.g. *Baker*, 2000; *Fennel*, 2001; *Iucci,* 2006; *Allen,* 2010], there is still a long way to go in order to understand the mechanisms of how space weather interacts with specific components and satellite systems [*Gubby et al.,* 2002]. The ability to quantify these effects requires the analysis of both space weather and satellite anomaly data [*Baker*, 2002; *Tretkoff,* 2010]. The main challenge is not access to space weather data, but rather satellite anomaly data.

Decades of spacecraft anomaly data sit unused in the electronic telemetry archives of major geostationary communications satellite manufacturers and operators. Telemetry comes from the Greek words tele (remote) and metron (measure), meaning to measure from a distance. These telemetry data are faithfully acquired and monitored by ground operators, and anomaly alarms are sounded should the component health data stray outside of pre-defined nominal or safe operational thresholds. The spacecraft health data are largely used in real time to help mitigate the effect of anomalies on the overall system performance and minimize impact to customers. Once the "fire" has been put out, the telemetry data are used for fault investigations, ground-based anomaly re-creation and modeling, and summaries of lessons learned.

The extensive databases of on-orbit anomalies from commercial spacecraft operators have not yet been released for scientific investigations. This is partly because scientific analyses of these anomaly data, beyond the engineering analyses for prompt detection and mitigation strategies, are not in the immediate interest of these businesses. Furthermore, in the commercial communications world, the challenge in predicting the effect of space weather events on communications satellites leads operators to continue nominal operation during periods of increased solar activity. However, these companies are interested in using accurate real-time space weather predictions and observations for fleet operations, and thus have some motivation to contribute via research collaborations with the space weather community.

In this work, we team with Inmarsat and Telenor, and potentially other operators, to analyze specific types of satellite component anomaly data to more accurately quantify the effect of space weather on geostationary communications satellites. More than 665,112 operational hours, or 500 MB, of Inmarsat on-orbit component telemetry and anomaly data, and more than 344,496 operational hours, or 6.5 GB, of on-orbit component telemetry and anomaly data for Telenor's satellite fleet has been obtained and will be analyzed.

1.2 Objectives

Other researchers have worked to understand more about any environmental mechanisms involved with satellite anomalies. However, much work remains in order to achieve an in-depth understanding of the specific types of space weather events that significantly impact component health, and the necessary methods for mitigating component failures [*Violet et al.*, 1993]. Understanding the causal relationship between space weather and component health is critical in improving the robustness of satellite hardware and thus improving the services that satellite operators provide to their customers.

The overall objective of this research is to investigate whether space weather effects are the likely cause of satellite component anomalies and which effects and causes of failure are the most likely candidates. Due to the fact that satellites are not returned to Earth for anomaly investigation, the actual cause of the individual anomalies is challenging to diagnose [*Choi et al.,* 2011; *Baker,* 2000]. However, the effects of high-energy particle radiation from relativistic electrons, low-energy electrons and high-energy protons, as well as galactic cosmic rays are suspected to play a major role [*Baker,* 2000]. Therefore, we will conduct a correlation analysis to better understand space weather's affect on spacecraft that should improve satellite design and reduce the maintenance cost for satellite operators.

Most studies of this nature analyze recorded spacecraft anomalies, verify the anomaly occurred, determine the time of the anomaly, and then compare the space environment for a period during and prior to the anomaly to determine if a relationship exists [*Violet et al.,* 1993]. This study follows in a similar manner for the analysis presented in Section 2.4: Study of Known Inmarsat Component Anomalies, and will help bring together the commercial satellite communications industry and space weather science communities to understand the sensitivity of key components to the changes of the space environment [*O'Brien et al.,* 2013]. The main goal is to improve both component robustness as well as system performance using design redundancy, operational, and predictive monitoring approaches.

1.2.1 Research Questions

The specific research questions that will be addressed are:

1. What are the future planned capabilities and design trends for geostationary communications satellites?
    a. How are satellite components, specifically power amplifiers, evolving with these trends?
2. How does the space environment, in terms of the low-energy electrons, the Kp index, high-energy protons and electrons, and galactic cosmic rays, affect current geostationary communication satellite components?
3. Can we use geostationary communication satellite telemetry to understand more about space weather phenomena in general and not just at the time of anomaly?

O'Brien et al. [2013] discuss the diverging development of priorities amongst space scientists and satellite operators. One example *O'Brien et al.* [2013] mention is that the scientific community places higher prioritization for forecasting, and significantly less priority for understanding the phenomena and particle populations of interest to the satellite operators. The proposed research questions will directly address this priority mismatch, and focus on investigating the space environment and understanding its effects on satellite systems with a goal of improving design of components and satellite operations.

1.3 Background

Space weather can impact the performance of satellite systems and can cause satellite anomalies [e.g. *Hastings et al.,* 1996; *Baker*, 2000; *Fennel*, 2001; *Iucci,* 2006; *Allen,* 2010]. When conducting analysis on the effects of space weather on satellite systems, it is of utmost importance to understand the satellite systems and components under investigation. Due to the demands for increased satellite capability, these components are progressively evolving, and the effects of space weather on state of the art components are often unknown until after they have flown. Additionally, advances in technology, particularly electrical component feature sizes, has increased complexity and reduced the size of the systems, which inadvertently has increased their susceptibility to the effects of space weather [*Baker*, 2000; *Wilkinson et al.*, 1991, 2000; *Gubby*, 2002].

In this Section 1.3: Background we discuss two primary topics. First, in Section 1.3.1: Trends in Geostationary Satellite Design, we discuss how the demands for increased satellite capabilities are causing design changes. Specifically, we look at how trends of increased power and data rates raise debates about which power amplifier technology, solid state power amplifier (SSPA) or traveling wave tube amplifier (TWTA), is best suited for geostationary communications satellite applications. Second, in Section 1.3.2: Space Weather Phenomena, we discuss the solar cycle, the Kp index, and energetic particle populations including electrons, protons, and galactic cosmic rays, and their known effects on satellite systems.

1.3.1 Trends in Geostationary Communication Satellite Design

Despite market doubts and bankruptcies of several commercial satellite companies in the 1980's and 1990's, telecommunications represents the most important commercial satellite application today, and is projected to grow in the future to accommodate high demand of video and multimedia content distribution [*Aloisio et al., 2010*]. Current trends of geostationary communication satellite designs are evolving. Among the trends are demands for higher bandwidth, data rates, smaller process features, higher power satellites, higher efficiency components, and reduced mass and size [*Robbins et al.,* 2005; *Rapisarda et al.*, 2010; *Murthy et al.,* 2011; *Bijeev et al.,* 2011]. The motivation behind these advancements focuses on enabling more information to be processed and sent at faster rates. As such, communication technologies are adapting to these demands. However, as the requirements for spacecraft capabilities grow, the satellite systems become more susceptible to environmental effects [*Baker,* 2000; *Denig et al.*, 2010]

Increasing the payload bandwidth and power utilization requires reconfiguration of the RF power across different beams and channels. Reconfigurability utilizes flexible payloads, such as flexible traveling wave tube amplifiers (TWTAs), which are capable of redistributing available power in the event of traffic imbalances between multiple beams over time. In designing with reconfigurability in mind, the payload must efficiently combine coverage, power, and bandwidth flexibility while reducing power consumption and cost [*Rinaldo*, 2005; *Aloisio et al.,* 2008]. This can pose major engineering and operational challenges.

Aloisio et al. [2010] enumerate several other key challenges and questions for the satellite broadband service providers pertaining to customer demands and system development:

- Traffic development is occurring non-uniformly, and current systems deal with this either inefficiently or without flexibility.
    - Can we design flexible and efficient payloads to cope with non-uniform traffic loads?
- Ka-band can individually support both interactive and broadcast data services.
    - Can we economically develop flexible multi-mission satellites?
- Users require enhanced interactive services for current price values.
    - Can satellite communications cope with this evolving user demand?

All of these challenges and questions relate to one important satellite requirement, power. Improving the power of a communications satellite requires improving the primary amplifier technologies, traveling wave tube amplifiers (TWTAs) and solid-state power amplifiers (SSPAs) [*Rapisarda et al.*, 2010]. These devices consume more than 80% of the satellite power; therefore maximizing their efficiency is critical [*Strauss,* 1994]. Increasing demand for higher power satellites with more amplifiers at higher output powers and more frequencies makes TWTAs historically the logical amplifier choice, as traditional SSPA technology at equivalent power and bandwidth levels has previously been unavailable [*Weekley and Mangus,* 2005; *Robbins et al.,* 2005]. However, recent technological advancements such as linearization and the implementation of different technologies such as GaN devices, have leveled the playing field. Additional comparisons and analysis of amplifier characteristics given the new technologies available are now necessary during the design process [*Strauss,* 1994; *Kaliski*, 2009].

1.3.1.1. What are power amplifiers? Why are they important?

RF power amplifiers are one of the key components of geostationary communication satellite technology, and are used to increase the power of a signal once received from the ground, then retransmit the signal down to a different specified location [*Robbins et al.,* 2005; *Kaliski*, 2009; *Strauss*, 1993]. Generally speaking, the satellite downlinks the signal to a user terminal on Earth. The purpose of these amplifiers is to process all earthbound signals to ensure that transmitted information is accurately relayed. In doing so the amplifier units consume 80-90% of the spacecraft bus power [*Illokken*, 1987; *Strauss*, 1993]. Therefore, amplifier efficiency is of utmost importance, and directly affects spacecraft sizing, payload capability and ultimately the total spacecraft mass [*Strauss,* 1993; *Kaliski*, 2009]. In the 1980s, C-band amplifier technology was capable of a power output of 8-16 Watts and Ku band amplifier technology was able to produce an output power of two to three times higher [*Strauss,* 1993]. Now they are able to operate at more than 200 Watts [*Rapisarda et al.*, 2010]. These technologies have experienced rapid change over the past several decades, and will undoubtedly continue to adapt to user demands and requirements.

1.3.1.2. Traveling Wave Tube Amplifiers

Traveling Wave Tube Amplifiers, or TWTAs, were the first successful RF power transmitting amplifier technology for communication systems, and were extensively used in satellite payloads at the birth of the space age in the 1960s [*Strauss,* 1993; *Mallon*, 2008]. L-3 Communications Electron Technologies, Inc. (ETI), formerly Hughes Aircraft EDD and then Boeing EDD, has been one of the leaders in TWTA development for satellite operations since 1963 with the launch of Syncom II. Since that time, TWTAs have advanced tremendously due to the increasing demand for higher power capabilities, greater bandwidth and higher data rates [*Robbins et al.*,

2005]. Design changes focus on increasing RF power output, efficiency and packaging compactness [*Bijeev et al.*, 2011].

TWTAs consist of a traveling wave tube (TWT) and an electrical power conditioner (EPC). A TWT is a vacuum electron device used to amplify the RF signal, and requires a conditioned power source [*Komm et al.,* 2001]. The main concern around the TWTA design is TWT performance, and assuring RF performance for 15-20 year operational lifetimes [*Strauss,* 1993; *Bijeev et al.,* 2011]. The EPC supplies regulated power to the TWT so that the RF performance is independent of seasonal variations (e.g. periods of sunlight and eclipse). Further, the EPC consists of several components such as DC-DC and DC-AC converters, protection circuits, and telecommand-telemetry circuits [*Bijeev et al.,* 2011].

Figure 1 [*Illokken,* 1987] shows the evolution of RF power output of TWTs in the 4 GHz to 20 GHz frequency spectrums (S Band to K Band) from 1970 to 1985.

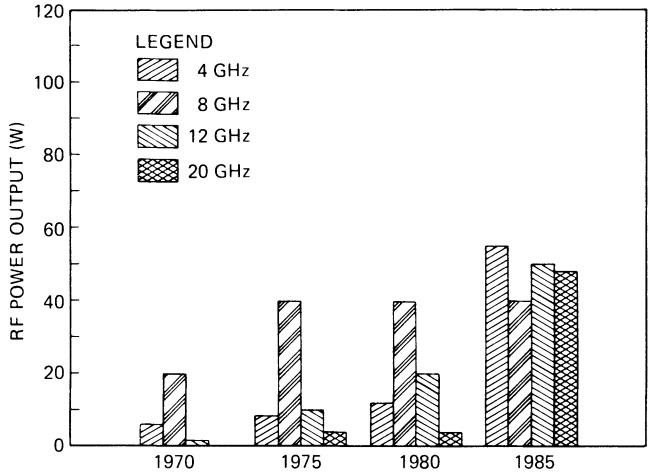

Figure 1: Evolution of levels in space TWTs [*Illokken*, 1987]

As shown in Figure 1, The RF power output from 1970-1985 increased from approximately 5 Watts to 50 Watts (1000%) for 4 GHz and similarly 12 GHz and 20 GHz. The major increase in RF power output for 8 GHz occurred between 1970 and 1975, when it experienced a 100% increase, but remained at 40 Watts between 1975-1985.

Five years later, in 1990, 32 GHz TWT space technology was at 10 Watts and 41% efficiency, and was used for NASA Deep space missions including Cassini (Ka-band frequency spectrum not included in Figure 1) [*Robbins et al.,* 2005]. Other TWTAs were capable of approximately 50-54% efficiency, compared to the SSPA alternative with 35% efficiency. At that time Ku-band TWTAs had 50 Watt power output, similar to the lower frequency TWTA technologies in 1985 shown in Figure 1, with efficiencies between 55-59% [*Strauss,* 1993].

In 2005, space TWTAs were operating across L band through Ka band with output powers between 15-150 Watts. Two specific examples of space TWTs at this time are the L-3 999HA and the 993H; these two models have instantaneous bandwidth as wide as 9 GHz, RF power from 50-250 Watts with efficiencies exceeding 61%. Interestingly, TWTA RF output power

increased more than 500% and efficiencies had increased more than 70% at C and Ku-band [*Robbins et al.*, 2005].

As TWTA technology developed, the concept of flexible TWTAs, or flex-TWTAs, with adjustable RF output power was introduced. Flex-TWTAs utilize a telecommand to modify the amplifier's anode voltage, or bias conditions, which provides a range of TWT output power [*Aloisio et al.,* 2008]. Varying the anode voltage yields a different cathode current, which produces a different TWT gain and output power. Flex-TWTAs enable methods for power conservation, which is beneficial for the overall mission as it can reduce the size or enable additional satellite capabilities [*Kaliski*, 2009].

In 2012, L3 ETI produced flight qualified L-band linearized TWTAs for communication satellites with 65% efficiency generating 140 Watts of output power at 1540 MHz. This TWTA, the L2000HBZ, was the highest efficiency L-band amplifier for space applications at the time, and produced three times the output power as the state of the art SSPA in 2012. The TWT component of the L2000HBZ provides a CW saturated RF output power greater than 200 W over a bandwidth of 50 MHz within 1.2-1.9 GHz (L band). Incorporating minor changes, the L2000HBZ can produce 300 W at S-band with greater than 72% electrical efficiency [*Feicht et al.,* 2012]. Another recent advancement in TWTA technology, also designed and fabricated by L-3 ETI, is the V band (50-75 GHz) 1693HD TWTA. As of 2012, this TWTA was the highest frequency, space-qualified TWTA, and was capable of producing more than 75 W of continuous wave (CW) saturated RF power. It also produces twice the bandwidth, better efficiency and linearity, as well as lower noise, mass and size than other leading V-band amplifiers [*Robbins et al.,* 2012].

1.3.1.3. Solid State Power Amplifiers

In the late 1970s, SSPA technology became available for space applications, and in the 1980s, SSPAs at an RF output power of 5-10 Watts became a successful alternative to the TWTA. SSPAs consist of an electrical power conditioner (EPC) and field effect transistors (FET). The FET is the component that provides the RF power amplification, and is generally Gallium Arsenide. While SSPAs were considered the amplifier of choice for some in the 1980's, an interesting change took place in 1990 when three spacecraft were equipped with 16 Watt, C-band TWTAs based on efficiency levels. Regardless, the use of SSPAs continued being used for higher power levels (20-40 Watts) despite having lower efficiencies than TWTAs [*Strauss,* 1993].

As the 1990s progressed, the SSPAs vs. TWTA debates primarily existed for systems that demanded 20 Watts or greater, but was still in support of SSPAs even at an output power of only 40 Watts. This preference was, and continues to be because of risk in the life-limiting thermionic vacuum device of the TWT [*Weekley and Mangus*, 2005]. SSPAs were also often chosen for their comparatively reduced mass [*Strauss*, 1994].

In 2000, SSPAs were operating in low frequency bands, such as L, S, and C, and were capable of achieving output powers of 30 Watts [*Escalera et al.*, 2000; *Robbins et al.*, 2005]. Furthermore, at this time the highest Ka-band SSPA was capable of an output power greater than 30 W with

20% power added efficiency (PAE) at 31 GHz with a linear gain of 52 dB. This Ka-band SSPA was considered to be a replacement for the TWTA [*Escalera et al.,* 2000].

1.3.1.4. SSPA vs. TWTA Space Technologies

Since the initial implementation of the SSPA in the 1970s, there have been debates as to which amplifier technology, TWTA or SSPA, is best suited for communication satellite applications. Arguments regarding these two satellite components generally pertain to amplifier reliability, performance, cost, and mass [*Strauss,* 1993; *Kaliski,* 2009]. Conducting an accurate comparison of the two technologies can be difficult, as there are numerous frequency bands and power requirements where no comparison can be conducted (e.g. SSPAs at very high power and high frequencies do not always exist) [*Kaliski*, 2009].

At one point, operation at C-band with an output power of 14-30 W was a regime in which both SSPAs and TWTAs operated, and thus in which a comparison could be made. Now, required power levels are at least 65 Watts, which traditionally would imply the use of TWTA technology, however recent advancements of SSPAs may prove otherwise [*Kaliski*, 2009]

TWTA supporters believe that TWTAs are the hardware of choice for space based communication systems because they are capable of providing high power at high frequency with better linearity and efficiency than competing alternatives. They also note that the ever-increasing demands of higher data rates and greater bandwidth make the TWTA technology the ideal choice for downlink amplifier applications [e.g. *Komm et al.,* 2001; *Robbins et al.*, 2005; *Bijeev et al.*, 2011]. Between 1992-2006, 69% of the geostationary communication satellites launched used TWTAs exclusively [*Mallon*, 2008]. TWTAs, like the L2000HBZ, are ideal when high power outputs are required, and are advantageous over SSPAs in regards to power output and low-waste heat loads for satellite operations [*Feicht et al.*, 2012; *Kaliski*, 2009]. *Mallon* [2008] states that the TWTA market share is beginning to overcome the SSPA market share because of the available TWTA reliability and performance.

Others strongly disagree and suggest that SSPAs have advantages in reliability, ruggedness, complexity, safety, size and cost compared to TWTAs, especially at microwave frequencies [*Escalera et al.,* 2000; *Sechi*, 2009]. Historically, SSPAs have been used at lower frequencies such as L and S band where their mass proved advantageous over TWTA capabilities [*Kaliski,* 2009].

The majority of power amplifiers live beyond their expected life of 15-20 years. However, amplifier failures do occur. SSPA technology supporters often doubt TWT reliability; traveling wave tube (TWT) failures, if they occur, are often due to interface problems, poor workmanship or material defects, and have tremendous impact on the satellite systems [*Illokken*, 1987]. A single failure can range from gradual power degradation to sudden unexpected switch off. TWTAs can take long periods of time, on the order of months to years, to fail, but may also experience a spurious switch off (SSO) due to voltage breakdown. SSPAs tend to fail unexpectedly [*Strauss,* 1993].

Even though debates over amplifier technologies have existed for decades, prior to 1990, there had been very few peer-reviewed published studies comparing SSPAs and TWTAs. Since then,

only three major studies have been published, which attempted to compare the capabilities of the two technologies. These studies took place in 1991, 1993 and 2005. The 1991 study was funded by the European Space and Technology Center (ESTEC) and focused primarily on the C-band frequency spectrum. In 1993, NASA sponsored an updated study expanding on the 1991 ESTEC study, and lastly [*Strauss,* 1993; 1994], in 2005 Boeing supported a study comparing SSPAs and TWTAs as well [*Weekley and Mangus,* 2005].

To elaborate further on each of the studies, in 1991 the ESTEC investigated C-band TWTAs and SSPAs; the results of the study were limited in distribution. Interestingly, prior to this study there were ample TWTA reliability data available, but little SSPA reliability data available [*Strauss,* 1994]. This study analyzed 75 spacecraft from eleven satellite entities, operating for more than 463 years, equipped with 1765 TWTAs (Ku and C band) and 309 SSPAs (C-band). The study found that RF power output levels and gains were similar, and that the amplifier failures did not provide additional explanation of failure mechanisms [*Strauss*, 1993]. Reliability was measured using redundancy analysis and manufacturer specified failures per billion amplifier-operating hours (FITs), and was used in payload design stages. TWTAs were found to be more reliable in the sense that SSPAs experienced 790 FITS, and TWTAs experienced 680 FITS. However, when evaluating redundancy there was 6/5 level redundancy for SSPAs and 3/2 for TWTAs, suggesting that TWTAs are less reliable [*Strauss*, 1994].

Two years later, NASA conducted additional analysis involving a group of 72 satellites, with 497 years of operations. Of these satellites the number operating at C-band increased 25%, from 962 in 1991 to 1220 in 1993. Interestingly, at the time C-band payloads were adopting SSPAs for 20-40 Watt RF power output requirements, such as Intelsat VIII, and for TWTAs for 50-70 Watt RF power output requirements. This study similarly found that SSPAs, while higher performing, reliable devices, were not as reliable as TWTAs, which were found to be 1/3 more reliable in the expanded study. The failure rates were found to have increased by 8% at Ku band with an output power of less than 65 Watts; statistics for greater output power were not available at the time of this study [*Strauss,* 1993].

Lastly, in 2005, *Weekley and Mangus* [2005] of Boeing analyzed 28.7 million hours of on-orbit C-band SSPA data and 148.6 million hours of on-orbit Ku-band TWTA data since the 1980's. Similar to the 1991 and 1993 studies, this study also incorporates FITS, highly proprietary to Boeing, to assess reliability of the amplifier components. Based one the large dataset, Boeing found no significant difference in reliability for TWTAs and SSPAs, but that observed FITs on the TWTAs are significantly less than the SSPAs. The SSPAs analyzed provided 66 Watts of output power less than the TWTAs, and therefore have different downlink capability. In terms of downlink, the TWTAs provided more than 6x the performance of the SSPAs. *Weekley and Mangus* [2005] also note that SSPA technology, with appropriate weight and efficiency, was simply not available for the high power and high frequency demands.

The three studies, published in 1991, 1993, and 2005 suggest that TWTA technology is more reliable than SSPA, but that SSPAs are often more advantageous in terms of mass. *Strauss* [1993] states that for output power of 15 – 50 Watts, either technology can be implemented, but that at higher frequencies (Ku and Ka band), TWTAs are historically more common.

Since 2005 there has not been another in depth study on the advantages of current TWTA vs. SSPA technologies. Therefore, we will analyze the SSPAs and TWTAs aboard the Inmarsat and Telenor satellite fleets, and will potentially include amplifiers aboard other satellite fleets as well. A description of our approach for this study is provided in Section 2.3: Study of Power Amplifier Design Trends.

1.3.2. Space Weather Phenomena

With the exception of Galactic Cosmic Rays (GCR), space weather originates from the sun, which emits solar flares, coronal mass ejections (CMEs) and produces corotating interaction regions (CIRS) that drive high-speed solar winds. When these disturbances reach Earth they can produce geomagnetic storms capable of causing hazardous anomalies (noise or even loss in telemetry, degradation to solar arrays, electrical upsets, etc.) and can also drastically diminish the quality of science data [e.g. *Baker,* 2002; *Cole,* 2003; *Barbieri et al.*, 2004].

CMEs result from the eruptions of the solar flares and usually occur more frequently during solar maximum [*Wilkinson*, 1994]. CIRs form in response to fast solar wind interacting with slower solar wind, and occur often show a 27-day periodicity [e.g. *Denton et al.,* 2006; *Tsurutani et al.,* 1995]. While seemingly similar, CMEs and CIRs uniquely alter the space environment and are primary sources of geomagnetic storms [*Kamide et al.,* 1998]. CIRs are associated with high-speed solar wind resulting in geomagnetic storms, which tend to occur during the declining phase of the solar cycle, These storms are usually longer in time, are associated with fluctuations in solar wind Bz component of the magnetic field, and are usually associated with the strongest increases in high-energy electrons in the outer radiation belt [*Li et al.,* 2005; *Miyoshi et al*., 2008]. These relativistic electrons produce higher levels of deep dielectric charging than CMEs [*Denton et al.,* 2006]. Interestingly, the bulk of internal charging anomalies at GEO occur during the declining phase of the solar cycle [*Wrenn and Smith,* 1996].

Spacecraft charging occurs when surrounding plasma particles bombard the satellite, and can deposit charge onto the surface of the satellite, or even penetrate the satellite shielding and deposit in the internal components. Once a build-up of charge accumulates beyond the material's breakdown potential an electrostatic discharge (ESD) occurs and emits lightning-like energy that can cause single event upsets (SEUs) or component anomalies in electronic systems [*Hastings et al.,* 1996; *Fennel et al.,* 2001, *Baker*, 2002; *Bodeau,* 2010].

1.3.2.1. The Solar Cycle and Solar Wind

The sunspot number, a metric derived from the observations of individual sunspots and groups of sunspots, is used to assess the overall strength and variability of solar activity. The increase and decrease in the sunspot number defines the maximum and minimum of the solar magnetic activity cycle, a period of approximately eleven years [*Hastings et al.,* 1996]. At solar maximum there is an increased chance of solar flares and CMEs, yet even at solar minimum, the Sun can produce damaging storms [*Allen,* 2010; *Cole*, 2003; *Baker,* 2000].

Solar wind density and speed are one of the key factors that determine the response of the magnetosphere to geomagnetic disturbances. The direction of the interplanetary magnetic field (IMF) plays a very important role. When the direction of the IMF is southward energetic solar wind particles can enter the Earth's magnetosphere and produce geomagnetic storms, which in

turn affects hardware performance and reliability. [*Cole*, 2003; *Riley,* 2012]. Furthermore, statistics have shown that anomalies in GEO tend to increase with geomagnetic activity [*Iucci et al.,* 2006].

Solar wind varies in density, temperature, and pressure. Average solar wind values are ~200-2,00 km/s and density of tens of particles per cm^{-3} [*Hastings et al.,* 1996]. In calm solar wind activity, the outer radiation belt, which traps energetic electrons (> hundreds of keV), is located between ~2.5 and 7 R_E, and the inner belt, which traps energetic protons (>10 MeV) and electrons, is between 1.2 and 2 R_E [*Schulz and Lanzerotti*, 1974]. Active solar wind activity can cause these regions to change in location and intensity, and can significantly compress the magnetopause. When solar wind compresses the magnetopause, or the boundary of the magnetosphere, past GEO, or to less than 6.6 R_E (36,000 km), it leaves geostationary orbits exposed to direct influence of the energetic particle populations that are present in the solar wind.

1.3.2.2. Low Energy Electrons

Low-energy electrons, on the orders of tens of keV, originate in the inner magnetosphere from magnetotail injections and drift eastward into the night portion of the magnetosphere [e.g. *Wrenn,* 1995; *Allen*, 2010 and references therein]. The strongest injections are produced by substorms. These particles deposit on the surface of the satellite, but do not possess enough energy to penetrate shielding materials [*Hastings et al.* 1996]. Several geostationary satellites have experienced anomalies due to surface charging; for example, the Maritime European Communications Satellite A (MARECS-A) experienced an uncommanded switching anomaly from a sudden increase in moderate energy electrons [*Wrenn,* 1995; *Baker,* 2000; *Koons et al.,* 2000]. Furthermore, it is widely acknowledged that surface charging anomalies generally occur between local midnight and dawn. [e.g. *Wrenn,* 1995; *Fennel et al.* 2001; *Lanzerotti et al.,* 1998; *Allen*, 2010]. We will also conduct local time analysis of the satellite anomalies to understand the distribution of local time at which the anomalies are occurring.

1.3.2.3. The Kp Index

The Kp magnetic disturbance index is often used as a proxy to quantify the relationship between surface charging and magnetosphric convection [*Gubby et al.,* 2002; *Thomsen*, 2004] that causes low energy electron enhancements near geostationary orbit [e.g. *Fennel et al.* 2001; *O'Brien,* 2009; *Choi,* 2011]. The Kp index represents the short-term geomagnetic disturbances caused by variations in the solar wind. The scale of Kp goes from zero to nine with zero representing a geomagnetically quiet environment and nine representing the most extreme geomagnetic environment [*Hastings et al.,* 1996]. Furthermore, between 1996 and 2012, only 2.2% of the Kp measurements were recorded as greater than a Kp of five, or as severe geomagnetic activity. *Reeves et al.,* [2003] notes that the disturbance storm time index (Dst) is not well related to relativistic particles or to the surface charging population.

1.3.2.4 High Energy Electrons

Most commonly 2 MeV electron flux is used as the representative electron spectrum capable of penetrating spacecraft structures [e.g. *Love et al.,* 2000; *Gubby et al.,* 2002]. These relativistic electrons are accelerated during geomagnetic storms and deposit into the dielectric materials of the satellites (semiconductors and circuit boards). If the rate of charge build-up exceeds the rate

at which charge can escape from the internal components an ESD or arcing will occur [e.g, *Hastings et al.*, 1996; *Shea et al.*, 1998; *Baker,* 2000; *Fennel et al.,* 2001; *Bodeau*, 2010; *Lai,* 2012]. Internal charging generally occurs one to several days after a major magnetic storm [*Baker,* 2000; *Koons et al.,* 2000].

The anomalies on ANIK E1, ANIK E2, the Japanese BS-3a satellite, Intelsat K, Galaxy 4, and Telstar 401 have been attributed in previous studies to internal charging [*Baker,* 2000; *Love et al.*, 2000; *Allen*, 2010; *Horne*, 2013]. However, at the time of the ANIK and Telstar anomalies the 2 MeV electron flux was very weak [*Baker,* 2000]. Interestingly, however these anomalies experienced periods of high flux levels of energetic electrons one to two weeks before the anomalies occurred [*Shea et al.* 1998; *Love et al.,* 2000].

1.3.2.5 High Energy Protons

High-energy protons, or solar energetic protons (SEPs), originate from CMEs and those of energies greater than 10 MeV can pose major challenges to satellite operations. In less than two days after the CME, these particles penetrate the Earth's magnetic field at the poles, crash into atmospheric particles, and produce ion and electron pairs that temporarily increase the plasma density in the lowest regions of the ionosphere [*Baker*, 2000; *Baker*, 2002]. This causes absorption of short wave radio signals and widespread blackout of communications, sometimes called a polar cap absorption event. Dangerous levels of high-energy particle radiation build up in the magnetosphere; this radiation can damage spacecraft microelectronics and pose a serious threat to the safety of astronauts. Energetic proton events can cause increased noise in photonics, total dose problems, single event upsets, and solar panel degradation.

Solar array degradation occurs primarily from radiation damage of solar proton events and galactic cosmic rays, and is one of the leading causes of decreased satellite performance (along with charging and SEUs) [*Koons et al.,* 2000]. Often, the design method to compensate for this degradation is to oversize the solar arrays, yet this solution is wasteful in terms of material and cost [*Hastings et al.,* 1996]. Thus causal relationship between high-energy protons and solar array degradation is of particular interest to the communications satellite industry as these interactions are not well understood, but drive cost and limit available power and fuel to sustain mission operation [*Barbieri et al.,* 2004].

1.3.2.6 Galactic Cosmic Rays

Galactic Cosmic Rays (GCRs) are the second type of particles that can cause SEUs and solar array degradation. GCRs consist mostly of protons (84% hydrogen) along with alpha particles (15% Helium) and less than 1% of heavier nuclei, and result from supernova explosions that spread cosmic rays [*Baker*, 2000; *Wilkinson et al.*, 1991]. These rays have energies up to 10^{14} MeV and occur out of phase with the eleven year solar cycle; the radiation from GCRs peaks at solar minimum and reaches a minimum at solar maximum [*Riley*, 2012; *Wilkinson et al.*, 1991, 2000]. At solar minimum, the solar winds are low and allow GCRs to reach the magnetosphere. This does not usually occur at solar maximum because the solar winds inhibit the GCRs from entering a trajectory towards the magnetosphere and the geostationary satellites. GCRs are monitored by cosmic ray detectors, which are most commonly in the form of ground-based neutron monitors [*Wilkinson et al.,* 2000].

2. Approach

The approach for this study is broken into six primary sections. First, we discuss how we have acquired specific environmental data sets, as well as how we plan to gather additional space weather data. Second, we discuss the satellite telemetry we have obtained. Followed by our approach for conducting a study on power amplifier trends in communications satellite design, and how SSPAs and TWTAs have evolved due to demanding user needs. Fourth, we present our analysis on the Inmarsat SSPA anomalies, and our approach for conducting the same analysis on the Telenor satellites, as well as conducting additional analysis on solar array degradation for both fleets. Then we describe our methodology behind designing an algorithm that will help detect component anomalies and determine how to what accuracy communications satellite telemetry can provide information pertaining to activity in the space environment. Lastly, we discuss the plan for progression of this work over the next 2.5 years.

2.1 Acquiring Space Weather Data

Observations of the space environment covering complete solar cycles are widely available. The OMNI2 data set is the primary space environment data set used in this study, and was obtained from the GSFC/SPDF OMNIWeb interface at http://web.gsfc.nasa.gov. OMNI2 contains hourly measurements of near-Earth solar wind magnetic field and plasma parameters, as well as Kp index, Disturbance Storm Time index (Dst), auroral electrojet (AE), and proton flux values. The OMNI2 data comes from numerous satellites such as the Advanced Composition Explorer (ACE) satellite, the International Monitoring Platform (IMP) satellites and the Geostationary Operational Environmental Satellite (GOES), as well as from the Data Analysis Center for Geomagnetism and Space Magnetism at Kyoto University in Japan [*King*, 2004].

High-energy electron flux data were obtained from two sources: Los Alamos National Labs (LANL) and GOES. The 1.8-3.5 MeV and 3.5-6 MeV electron flux data were obtained from the LANL GEO Energetic Sensor for Particles (ESP). These values are daily averages of the electron flux, and are shown to be nearly identical to the distribution of the GOES > 2 MeV electron flux [*Reeves,* 2011].

We used the NOAA National Geophysical Data Center to obtain GOES Space Environment Monitor (SEM) data to gather 2 MeV integral electron flux and to assess relativistic electrons at the time of SSPA anomalies. This sensor suite has provided continuous magnetometer, particle and X-ray data since the mid-1970s, and is a primary source for public, military and commercial space weather warnings [*GOES*, 1996]. The GOES 2 MeV integral electron flux data, with a five second interval, was obtained from the GOES satellite longitudinally closest to the respective Inmarsat satellite that experienced the anomaly. Interpretation of results will keep these longitudinal separations in consideration. At any point between 1996 and 2012 at least two of the GOES 8 – GOES 15 satellites were collecting data. During this time, several of the GOES satellites were either decommissioned into a parking orbit or experienced technological difficulties and are thus not included in this study. Nonetheless, of the remaining GOES satellites, GOES 12 is the primary satellite used for gathering SEM data, GOES 8, 10, 13 and GOES 14 were also used when one of these satellites was located closer to the anomalous satellite and for dates outside of the and GOES 12 coverage time span. The SEM consists an energetic particle sensor/high-energy proton and alpha detector (EPS/HEPAD), which contains

two energetic proton, electron and alpha detectors (EPEADs), a magnetospheric proton detector (MAGPD), a magnetospheric electron detector (MAGED), and a HEPAD [*NSWPC*, 2007].

Sunspot data, including smoothed and raw sunspot numbers were obtained from the Solar Influences Data Analysis Center (SIDC) of the Royal Observatory in Brussels, Belgium. This data was used to plot the solar cycle over which the communications satellites were in operation to determine at what point the anomalies tend to occur.

As previously mentioned, GCR flux is generally monitored with ground-based neutron monitors. We are currently in the process of determining the best method and source for obtaining GCR data to compare with the geostationary communications satellites in our study. Past studies of similar nature have included GCR data from the Deep River neutron monitor in Canada [*Shea et al.,* 1998; *Wilkinson et al.,* 2000]. Once we have determined our data source, we will obtain GCR data from 1996-2012, the period in which the Inmarsat and Telenor satellites are operating.

2.2 Acquiring Geostationary Communications Satellite Data

While space weather data are widely available, access to satellite health data and information on anomaly occurrences is quite limited. Therefore to obtain the desired telemetry and satellite information, we collaborate with two satellite operators, Inmarsat and Telenor. We collaborate with Inmarsat, a telecommunications company based in the U.K., to analyze 665,112 operational hours, or more than 500 MB, of satellite telemetry data from eight satellites on two of Inmarsat's satellite fleets. There are five satellites in what we will call Fleet A and 3 satellites in Fleet B. We also collaborate with Telenor, a telecommunications company based in Norway, to analyze 344,496 operational hours, or more than 6.5 GB, of satellite telemetry from four unique satellites. The satellite telemetry databases are used to identify and investigate both nominal and anomalous satellite component performance. Data on amplifiers (SSPAs and TWTAs) and eclipse durations were obtained, along with solar panel data, anomaly lists and SEU information for each satellite. Table 2 describes the collected satellite telemetry.

Table 2: Telemetry Descriptions

Telemetry Parameter	**Description**
Amplifier Current	SSPA or TWTA current
Amplifier Temperature	SSPA or TWTA temperature
Total Bus Power	Instantaneous power of the main power bus, power values are calculated from prime and redundant voltage and current sensors on the main bus
Solar Panel Current	Output of the short-circuit cell current sensor located on the outboard panel of the north and south wing, used to determine when satellites are in eclipse
Solar Panel Voltage	Output of the open-circuit cell voltage sensor located on the mid-board panel of the north and south wing

Operators often classify the amplifier anomalies into two categories: "hard" failures and "soft" failures. Both types of failures are identified when spacecraft health telemetry, such as the SSPA current, fall below a pre-defined threshold. The threshold setting is specific to particular hardware; for example, the SSPA current thresholds for the satellite fleets are different, because

the configurations, manufacturers and/or model of these components are different. The spacecraft health measurements are continuously recorded (e.g., hourly) and saved and then downlinked to the ground where they are monitored and archived. All known anomalies present in the operators archive will be considered in this study.

When the amplifier is irradiated by high-energy particles that transfer more than the radiation ionization energy to the semiconductor, an electron hole pair forms in the semiconductor material (such as silicon or Gallium Arsenide GaAs) [e.g., *Alig et al*., 1975]. This changes the charge carrying capability and affects the amplification properties of the transistor of the amplifier, which can cause anomalies to occur [*Bhat et al.* 2005]. Similar to the two studies presented in *Strauss* [1993], and mentioned in Section 1.3.1.4: SSPA vs. TWTA Space Technologies, the Inmarsat SSPAs did not experience a single generic amplifier failure mechanism, but experienced abrupt unexpected switch-offs.

Of the twenty-six SSPA anomalies only four were soft failures, and 22 were hard failures. Only one of the SSPAs that experienced a soft failure was ultimately able to continue nominal operation. Thus 25/26 SSPA anomalies called for a redundant SSPA unit to be switched on. One of the twenty-six SSPA anomalies that called for a redundant SSPA unit did not have a replacement SSPA available because it had already been switched on from a previous anomaly. It is clear that a major performance degradation results when replacement SSPAs are unavailable if they are already in use. Similar to the two studies presented in *Strauss* [1993], and mentioned in Section 1.3.1.4: SSPA vs. TWTA Space Technologies.

The shielding and the mounting location of the satellite hardware play an important role in protecting components from the harmful effects of the space environment [*Strauss*, 1993]. SSPA units are generally mounted inside the satellite in an electronics box or chassis, where they can be monitored in a thermally controlled environment (thermal management of power amplifiers is a substantial part of communications satellite design). The SSPAs are also somewhat protected from space weather hazards via the external shielding of the spacecraft bus and shielding from other internal units. The typical shielding of a geostationary communications satellite is approximately 10 mil Al equivalent (or 0.254 mm of Al) for its solar arrays which typically surround the body of the satellite in addition to any deployed panels [*O'Brien*, 2009], and the internal shielding of SSPAs in communications satellites typically ranges between less than 1 mm Al equivalent to slightly more than 3 mm Al equivalent depending on the geometric distribution of the internal components. However, high-energy relativistic electrons (> 2 MeV) and galactic particles are capable of penetrating both types of shielding and can cause anomalies for internal components [*Hastings and Garret,* 1996].

It is relevant to note that Inmarsat has not had any extended service interruptions due to the SSPA anomalies. Satellite manufacturers incorporate redundancy into their design, so that when an SSPA anomaly occurs, a redundant SSPA is turned on to provide continuous operation at full capacity. However, as satellite lifetimes extend beyond design expectancies, which is becoming increasingly common and is also a profitable position to be in, there are fewer available redundant units with time, and thus satellites operating beyond their design lifetime may have more frequent outages.

It is interesting to have the opportunity to utilize spacecraft telemetry to understand the effects of the space weather environment, and compare like anomalies with environmental data enables pattern identification and the establishment of a plausible cause [*Wrenn*, 1995]. When possible, analyzing data from satellites of the same fleet, and then comparing the results with other fleets provides insight into both how space weather affects similar components and systems within each fleet as well as general trends that are common for different fleets. Such an approach is only feasible within a focused study and cannot be applied to a more general statistical analysis of different spacecraft anomalies.

2.3 Study of Power Amplifier Design Trends

We will analyze SSPAs and TWTAs aboard the Inmarsat and Telenor satellite fleets, and will potentially include amplifiers aboard other satellite fleets as well. Specifically we will analyze their capabilities (RF output power level, frequency, and efficiency) in comparison with historical satellite fleets in order to better understand the trends of amplifier technologies, and which amplifiers are preferred. We will also analyze amplifier reliability by investigating the telemetered operating current device at the time of, and periods of time prior to the amplifier failure.

Essentially, we will conduct a follow on study to the 2005 Boeing analysis described in Section 1.3.1.4: SSPA vs. TWTA Space Technologies. The 2005 Boeing study was not a correlation between RF power output capability or frequency and reliability, however, as mentioned, we plan to incorporate amplifier capability into our analysis. The first aspect of our study will explore current amplifier capabilities.

Weekley and Mangus [2005] found that 100% of the TWTA anomalies were in the Ku-band and that the SSPA anomalies were primarily in the C-band. The Inmarsat satellites in our analysis operate in Ka and L band, and the Telenor satellites operate in Ka band. Understanding the RF power output and frequency capability of the Inmarsat and Telenor satellites, and comparing them to the satellites included in the 1991, 1993, and 2005 studies will improve our understanding on the evolution of these devices.

Unfortunately projected FIT values are highly proprietary information for amplifier technologies. We will analyze the state or condition of the device at the time of failure by examining telemetry data, specifically amplifier current, prior to the anomaly and the age of the device at the of the anomaly. Elevated current levels prior to amplifier anomalies can help designate failure mechanisms and improve our knowledge of the types of failures occurring on these satellites.

Weekley and Mangus [2005] state that a single satellite component failure has essentially zero impact on the communications function. They find that more than 80% of the satellites in their study experienced zero TWTAs and SSPAs anomalies. Of the 20% of satellites that did experience SSPA anomalies, only 9% experienced more than two SSPA anomalies per satellite. Of the eight Inmarsat satellites alone, equipped with more than 450 SSPAs, 88% of the satellites experienced SSPA anomalies, 75% experienced two or more SSPA anomalies. A clear difference between the satellites described in the 2005 Boeing study, and the Inmarsat satellites exists. However, incorporating data from other communication satellites in operation will aid in validating our results.

Another important aspect to consider is that as technological capabilities evolve (e.g. with smaller feature sizes) the susceptibility of newer technologies to radiation will also increase [*Baker*, 2000; *Love et al.*, 2000; *Gubby et al.,* 2002]. A study comparing modern day TWTA and SSPA technology will help define performance levels at which both are competitive, and will improve the current understanding of the technological advancements of the devices since 2005 [*Kaliski,* 2005].

2.4 Study of Known Inmarsat Component Anomalies

Inmarsat has been operating its fleet of geostationary (GEO) satellites for more than twenty years, and has maintained a complete archive of component telemetry and housekeeping data for more than twenty years with the primary purpose of monitoring spacecraft health and performance. Since 1996, the satellites have experienced twenty-six solid-state power amplifier (SSPA) anomalies; individually, each satellite has experienced between zero and eight SSPA anomalies. We have conducted analysis on the Inmarsat fleets and will expand the Inmarsat analysis to incorporate Telenor data and broaden our current results. We discuss our preliminary analysis of the Inmarsat telemetry and discuss our plan to expand upon this work with our additional datasets in Section 2.4: Study of Known Inmarsat Component Anomalies.

Recently, *Choi et al.* [2011] analyzed the effects of space weather on ninety-five satellite anomalies from seventy-nine unique satellites archived in the Satellite News Digest (SND) between 1997-2009. The study noted relationships between anomalies and seasonal dependencies, satellite local time, geomagnetic index Kp, and charged particles observed by Los Alamos National Laboratory (LANL) satellites. The study suggested that energetic electrons might contribute to anomalies, but noted that the relationship between anomalies and electrons is not well established. *Mazur and O'Brien* [2012] commented on the data population of *Choi et al.* [2011] and emphasized the importance of a careful analysis of the anomaly records.

Similar to the study conducted by *Choi et al.* [2011], we will investigate relationships between anomalies and geomagnetic index Kp, magnetic local time, and seasonal dependencies. We will also analyze hazardous particle populations that may affect the components on the geostationary satellites including low-energy electrons, which can cause surface charging, and high-energy relativistic electrons, which can cause internal charging, and high energy protons and galactic cosmic rays, which cause single event upsets (SEUs) and solar array degradation [*Baker,* 2000, 2002; *O'Brien et al.,* 2013]. Our preliminary analysis does not support an association between the SSPA anomalies and solar flares, or strong ring current (large negative Dst) events [*Lohmeyer et al.,* 2012]. Therefore we do will not focus our analysis on solar flares or on Dst.

2.4.1. Inmarsat Solid State Power Amplifier Anomalies

Throughout a spacecraft's lifetime, component health and performance degrades as a result of exposure to space weather [*Baker,* 2000]. Satellite performance anomalies occur when a component operates outside of its defined threshold for nominal performance. Thresholds are established to monitor the health of components and notify operators when the component experiences anomalous performance. For amplifiers, the main threshold of concern is the amplifier current.

The SSPA current reflects the amplification capability of the device [*Robbins et al.,* 2005]. Over an undetermined period of time, continuous bombardment of energetic particles can deposit themselves into an amplifier's material and change the charge mobility that was originally determined by the dopant concentrations of an amplifier's material and thus leads to a change in conductivity that will affect current, which is a parameter monitored and tracked in housekeeping telemetry. If the current exceeds the upper threshold, the SSPA will saturate. The non-linear amplification past saturation is undesirable as it generates harmonics and distorts the transmitted signal. If the current falls below the lower threshold, then the SSPA will not provide enough current to adequately amplify the signal. Space weather effects can modify the operation and efficiency of the amplifiers and cause amplifier anomalies, which in turn will limit the operational lifetime of the satellite. *Weekley and Mangus* [2005] note 80% of SSPA failures disable downlink capabilities.

As previously mentioned, SSPAs consist of an RF amplifier and Electronic Power Conditioner (EPC). Depending on the application (orbit and expected lifetime) the devices may require spot shielding. Manufacturers perform ray tracing to quantify the amounts of shielding provided to individual components and their potential exposure to the radiation environment [*Schwank*, 2008]. In the event that spot shielding is required, precautions regarding component grounding are also taken. Satellite manufacturers measure grounding as a part of assembly, integration and testing. Due to the relatively high amounts of shielding used and the location of the SSPAs (deep within the spacecraft) we do not consider charging from substorm-injected electrons, which cause surface charging, as a primary issue for these SSPA units. However, we will still investigate surface charging as a potential component hazard in this study.

In the upcoming sections, Section 2.4.1.1 to Section 2.4.1.7, we discuss our analysis and future work investigating the SSPA anomalies and the solar cycle in Section 2.4.1.1, followed by Section 2.4.1.2: SSPA anomalies and Kp as a proxy for surface charging. Then we investigate SSPA anomalies and high-energy electrons as well as high-energy protons, and galactic cosmic rays in Section 2.4.1.3, 2.4.1.4, and 2.4.1.5 respectively. The last two sections describe the local time and seasonal dependencies of the SSPA anomalies.

2.4.1.1. SSPA Anomalies and the Solar Cycle

Figure 2 displays the smoothed sunspot number from Solar Influences Data Analysis Center (SIDC) of the Royal Observatory in Belgium and the Inmarsat SSPA anomalies between 1996 and 2012. The two Inmarsat satellite fleets, Fleet A and Fleet B, are designated with different colors. This period encompasses part of solar cycle 23 (May 1996 – Dec. 2008) and part of solar cycle 24 (Jan. 2009 – present). Solar minimum for Cycle 23 occurred in 1996, and the maximum for Cycle 23 occurred in 2002. The solar minimum for Cycle 24 occurred between 2008 and 2009; however, the solar maximum has yet to occur for Cycle 24 [*Riley*, 2012].

It is important to separately consider the effects of space weather on satellites as a fleet, as they are from different satellite manufacturers. This is because different components, geometries, shielding, and operational configurations will have different sensitivities to space weather. We can compare "identical" spacecraft within a particular fleet, but here refrain from drawing conclusions using combined data over a solar cycle. Rather, we should wait until we have

enough data such that each fleet has individually experienced a full solar cycle.

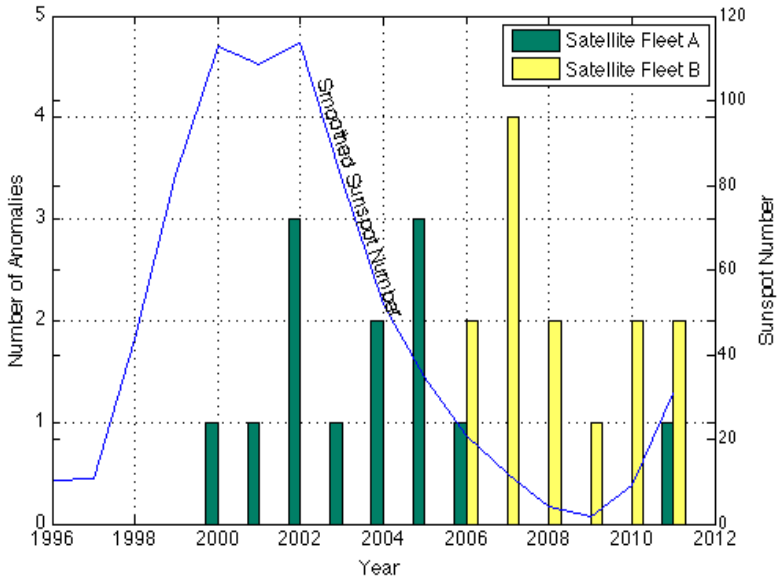

Figure 2. Yearly SSPA anomaly totals per Inmarsat satellite fleet, plotted with the smoothed sunspot number (blue line).

There were no SSPA anomalies for either fleet prior to 2000, even though this time period includes launch and the initial years of operation for several of the satellites. The initial operation period is commonly associated with satellite anomalies due to the hazards of the launch environment and orbital repositioning. For Fleet A, anomalies occur between 3.5 and 14.5 years of operation, whereas for Fleet B, anomalies occur from less than 0.2 to 7 years of operation. Therefore, the occurrence of the SSPA anomalies does not show a clear correlation with the satellite or amplifier age. It is interesting to also note that in Figure 2, Fleet A has far fewer SSPA anomalies around solar minimum than Fleet B does; this emphasizes the point that they should be considered separtely.

Figure 3 displays the number of SSPA anomalies per year per satellite in Fleet A, along with the solar cycle. A similar graph for Fleet B is not shown, because data for a full solar cycle does not exist. However, we will conduct this analysis for the Telenor satellites, of which two of the four have operated for an entire solar cycle.

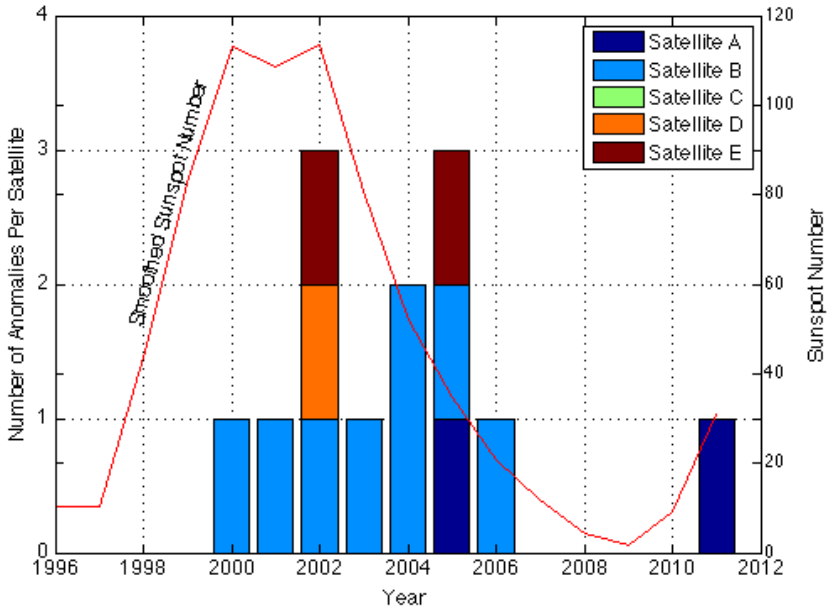

Figure 3. SSPA anomalies per year for Inmarsat Fleet A from 1996 to 2012, each letter in the legend corresponds to a different satellite in the fleet. This satellite fleet has data for an entire solar cycle, whereas Fleet B has not.

For Inmarsat Fleet A, no SSPA anomalies occur immediately after launch, or even within the first three years of operation. Therefore, analysis of launch telemetry indicates that the SSPA anomalies for Fleet A are not related to launch environment. Consistent with *Choi et al.* [2011]*'s* study, the SSPA anomalies on Fleet A do not primarily occur at solar maximum, when surface charging anomalies are most likely [*Denton et al.,* 2006], but occur during the declining phase of the solar cycle. As previously mentioned, the declining phase of the solar cycle is the time when CIRs drive high-speed solar wind streams and produce enhancements of relativistic electrons, notoriously known to cause internal charging [*Shea et al.,* 1998; *Wrenn et al.*, 2002; *Denton et al.*, 2006; *Miyoshi*, 2008]. Hot electron temperature, which has been found to determine surface-charging level also reaches a maximum during the declining phase of the solar cycle [*Denton et al.,* 2006].

The correlation between the distribution of the thirteen SSPA anomalies aboard Fleet A and the expected internal charging from energetic electrons may indicate that relativistic electrons played a role in causing the anomalies. It is still difficult to completely rule out other causes of anomalies, as there is limited statistical data. More statistical studies with space weather data and anomalies onboard satellites operating over an entire solar cycle will be required to validate the observed correlation and definitively establish the relationship between deep dielectric charging and SSPA anomalies.

2.4.1.2. SSPA Anomalies and Kp as a proxy for surface charging

Figure 4(a-h) shows the distribution of the Kp index from 1996-2012 for (a,b) every Kp measurement, (c,d) Kp averaged over two days, (e,f) Kp averaged over three days and (g,h) Kp averaged over two weeks, or fourteen days. The y-axis, labeled Count, represents the number of Kp measurements. The Kp distributions for Inmarsat Fleet A are shown in Figure 4(a,c,e,g). Each Fleet A anomaly is shown with a green square. The Kp distributions for Fleet B are shown

in Figure 4(b,d,f,h). Each Fleet B anomaly is shown with a cyan circle. The anomaly placement points are calculated using the respective averaging method of each figure. For example the anomaly points on Figure 4(c) represent the average Kp value of the two days prior to the anomaly. Each point represents a single anomaly. The vertical location of the point does not correspond to a count value, as labeled on the y-axis of each plot.

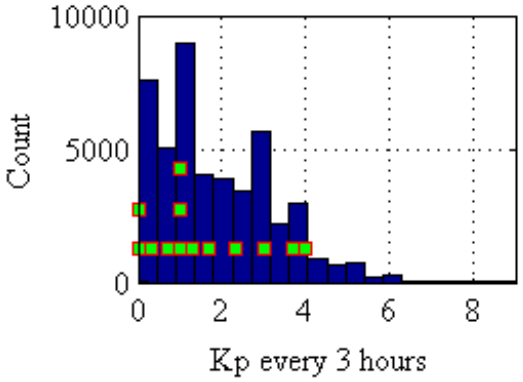

(a)

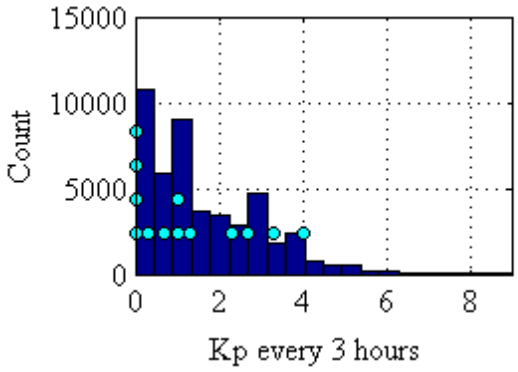

(b)

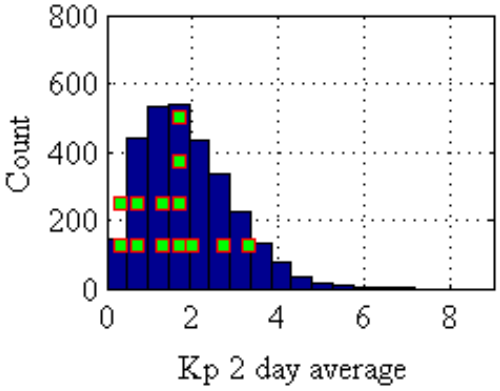

(c)

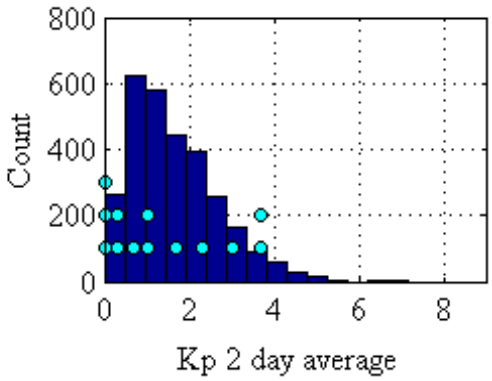

(d)

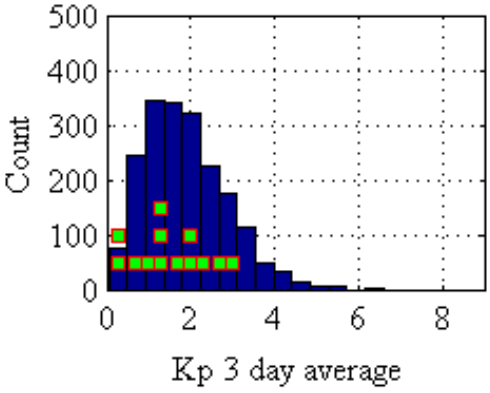

(e)

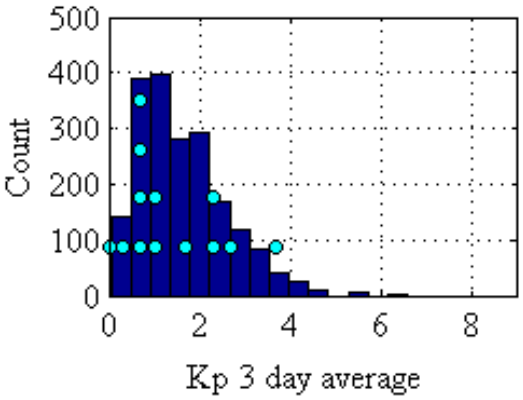

(f)

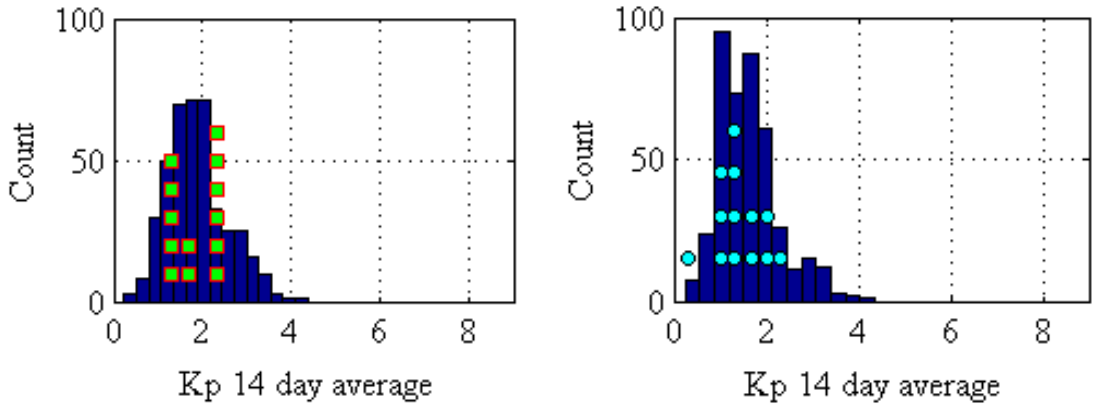

(g) (h)

Figure 4 (a-h). The distribution of Kp Index for (a,b) every measurement, (c,d) two day average, (e,f) three day average, and (g,h) two-week average with Kp index at the time of the SSPA anomalies. The distributions for the time period of operations of Fleet A are shown in Figure 4(a,c,e,g) and the anomalies of Fleet A are represented with green squares. The distributions for the time of period of operations of Fleet B are shown in Figure 4(b,d,f,h) and the anomalies of Fleet B are represented with cyan circles. The specific time periods of each fleet are not distinguished for proprietary reasons, but only include periods when the respective satellite fleets were in operation. The Kp time series are taken from the Data Analysis Center for Geomagnetism and Space Magnetism at Kyoto University in Japan and was accessed through the OMNI 2 web site.

The Inmarsat anomalies do not appear to depend on the Kp Index. Figure 4f, for example, shows more anomalies at small Kp values, and there appear to be more days with smaller Kp during the time of the operation of Fleet B. However, after normalizing results by the number of days in the time series with a given Kp value we found that anomalies do not preferentially occur for high Kp or low Kp values. Conducting this analysis with additional anomaly data from Telenor, and other operators, will help verify this preliminary conclusion. A summary of the four Kp distributions is provided in Table 2 for Fleet A and Table 2 for Fleet B. Interestingly, for both fleets the maximum Kp at the time of anomaly the did not exceed a Kp of 4. Twenty-one out the twenty-six (80%) anomalies occurred when the Kp was less than 2.5.

Table 2 and 3 summarize the mean Kp, the standard deviation of the Kp distributions, the minimum Kp and the maximum Kp for all four distributions. For Fleet A the average Kp of all anomalies for the four distributions is greater than the respective values for Fleet B, as the anomalies of Fleet B occur after 2006 when geomagnetic activity was low. The minimum and maximum Kp values at the time of the anomalies are approximately equal for both fleets.

Table 2: Fleet A Summary of Kp at time of Thirteen SSPA Anomalies

Fleet A	Kp	Kp 2 day average	Kp 3 day average	Kp 14 day average
Mean	1.538	1.542	1.567	1.848
Standard Deviation	1.335	0.832	0.828	0.425
Min. Value	0	0	0.449	1.287
Max. Value	4	3.248	3.097	2.326

Table 3: Fleet B Summary of Kp at time of Thirteen SSPA Anomalies

Fleet B	Kp	Kp 2 day average	Kp 3 day average	Kp 14 day average
Mean	1.277	1.427	1.387	1.406
Standard Deviation	1.371	1.320	1.110	0.540
Min. Value	0	0.072	0.138	0.256
Max. Value	4	3.656	3.776	2.386

To relate these results to charging phenomena, *O'Brien* [2009] found the probability of an anomaly caused by surface charging peaks in the Kp of 4-6 range, which is more than two times higher than the average Kp value at the time of the anomalies. Results thus far do not suggest that anomalies have a clear relationship with Kp, which is used as a proxy for low energy electron flux. This suggests that the anomalies occurred at times of relatively quiet geomagnetic activity, and that the anomalies are likely not caused solely by surface charging.

2.4.1.3. SSPA Anomalies and High Energy Electrons

Figure 5(a-d) shows the distribution of the $\log_{10}$ of 1.8-3.5 MeV daily averaged electron flux from 1996-2009 measured on LANL SOPA [*Reeves et al.,* 2011] for (a) every measurement, (b) averaged over two days, (c) averaged over three days and (d) averaged over two weeks, or fourteen days. The probability distribution of $\log_{10}$ of the 1.8-3.5 MeV electron flux at the time of the anomaly, approximated to the nearest 0.2 pfu, is shown for Fleet A with green squares, and Fleet B with cyan circles. Similar to Figure 4, the y-axis, Count, represents the number of measurements. For this data the measurements are daily electron flux values. The vertical location of the anomaly markers does not correspond to the count values on the y-axis. For Fleet B, five anomalies occurred when flux data from LANL is not available. Therefore, both fleets are shown on the same figure, rather than separated, which should be done for large data sets.

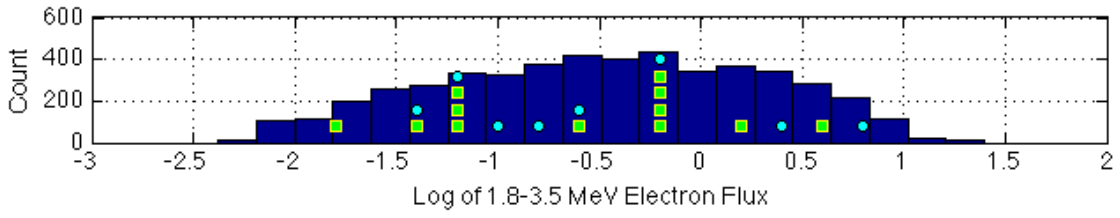

(a)

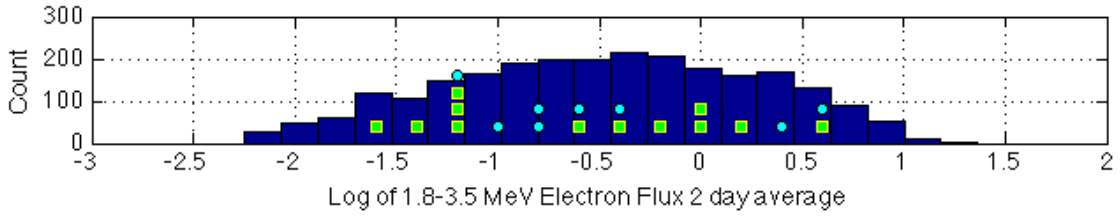

(b)

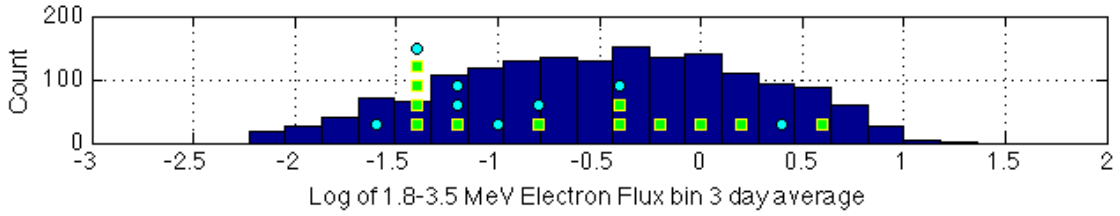

(c)

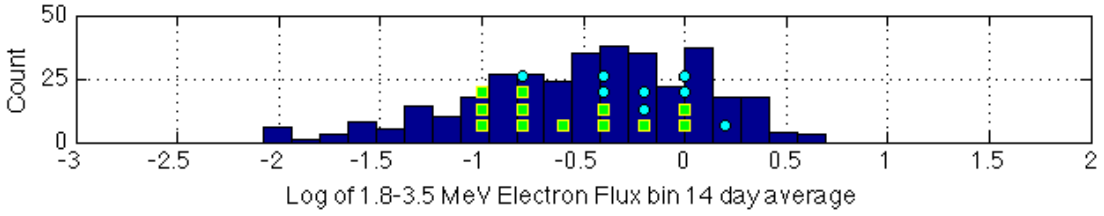

(d)

Figure 5 (a-d). The distribution of the $\log_{10}$ of 1.8-3.5 MeV Electron fluxes in units of #/(cm^2 s st keV) from 1996-2009 for (a) every measurement, (b) two day average, (c) three day average, and (d) two-week average with electron flux at the time of the SSPA anomalies on Fleet A (green squares) and Fleet B (cyan circles).

From 1996-2009, as LANL data is not available after 2009, the average log of 1.8-3.5 MeV Electron flux was -0.489 $\log_{10}$(#/(cm^2 s st keV)) with a standard deviation of 0.75 $\log_{10}$(#/(cm^2 s st keV)). Anomalies occur between $\log_{10}$ of electron flux values of -1.81 $\log_{10}$(#/(cm^2 s st keV)) and 0.55 $\log_{10}$(#/(cm^2 s st keV)) for Fleet A, and -1.47 $\log_{10}$(#/(cm^2 s st keV)) and 0.85 $\log_{10}$(#/(cm^2 s st keV)) for Fleet B. There does not appear to be an obvious, unique distribution of the electron flux at the time of the anomalies, however more satellite anomaly data will help clarify if a trend exists.

Interestingly, eleven of the twenty-six anomalies experienced elevated flux approximately one to two weeks prior to the anomaly. Elevated flux is defined as flux greater than one standard deviation above the average flux from 1996-2009, or a $\log_{10}$ of 1.8-3.5 MeV electron flux of 0.297. The average of the enhanced values that occurred prior to the anomalies was 0.7419 $\log_{10}$(#/(cm^2 s st keV)) or 1.57 standard deviations above the $\log_{10}$ of 1.8-3.5 MeV electron flux. Of the total 4949 electron flux measurements between 1996-2009, 229 measurements or (4.6% of the measurements) were above 1.57 standard deviations of the $\log_{10}$ of 1.8-3.5 MeV electron flux. These 229 measurements do not occur uniformly between 1996-2009. The 229 measurements are clustered around the declining phase of the solar cycle and are vary sparse at solar max. Therefore, to understand the likelihood that a random anomaly occurs one to two weeks after a level of $\log_{10}$ of 1.8-3.5 MeV electron flux greater than 1.57 standard deviations between 1996-2009 we conducted a Monte Carlo simulation. Specifically, we determined the likelihood that twenty-six random anomalies would occur between seven and fourteen days after a level of $\log_{10}$ of 1.8-3.5 MeV electron flux greater than 1.57 standard deviations. For 100,000 iterations of the Monte Carlo simulation we found that on average 2 out of 26 anomalies occur seven to fourteen days after a $\log_{10}$ of 1.8-3.5 MeV electron flux greater than 1.57 standard deviations. We find that about five times that number of anomalies occurred after elevated electron events of the same level in the data.

As previously mentioned, the Japanese BS-3a and the ANIK satellites also experienced enhanced levels of high-energy electron flux one to two weeks before an anomaly. *Wrenn* [1995] provides statistical, conclusive evidence that internal dielectric charging was the cause of the ANIK satellite failures. Therefore, one plausible cause of these eleven SSPA anomalies could be from internal dielectric charging. *Bodeau* [2010], however, suggests that long delays between electron enhancements and anomalies due to internal charging may not be likely. In future work we will continue to investigate whether anomalies result from the combined effect of internal charging by comparing additional anomalies with high energy particle populations, including GCRs.

Figure 6(a-d) displays the GOES 2 MeV electron flux rate (solid blue line) and the SSPA current (dotted green line) two weeks before and after four SSPA anomalies. The anomaly is designated with a red line. The periodic higher frequency variability in both the SSPA and 2 MeV data is due to the diurnal cycle. In Figure 6(a), the peak 2 MeV electron flux occurred 10.6 days before the SSPA anomaly occurred.

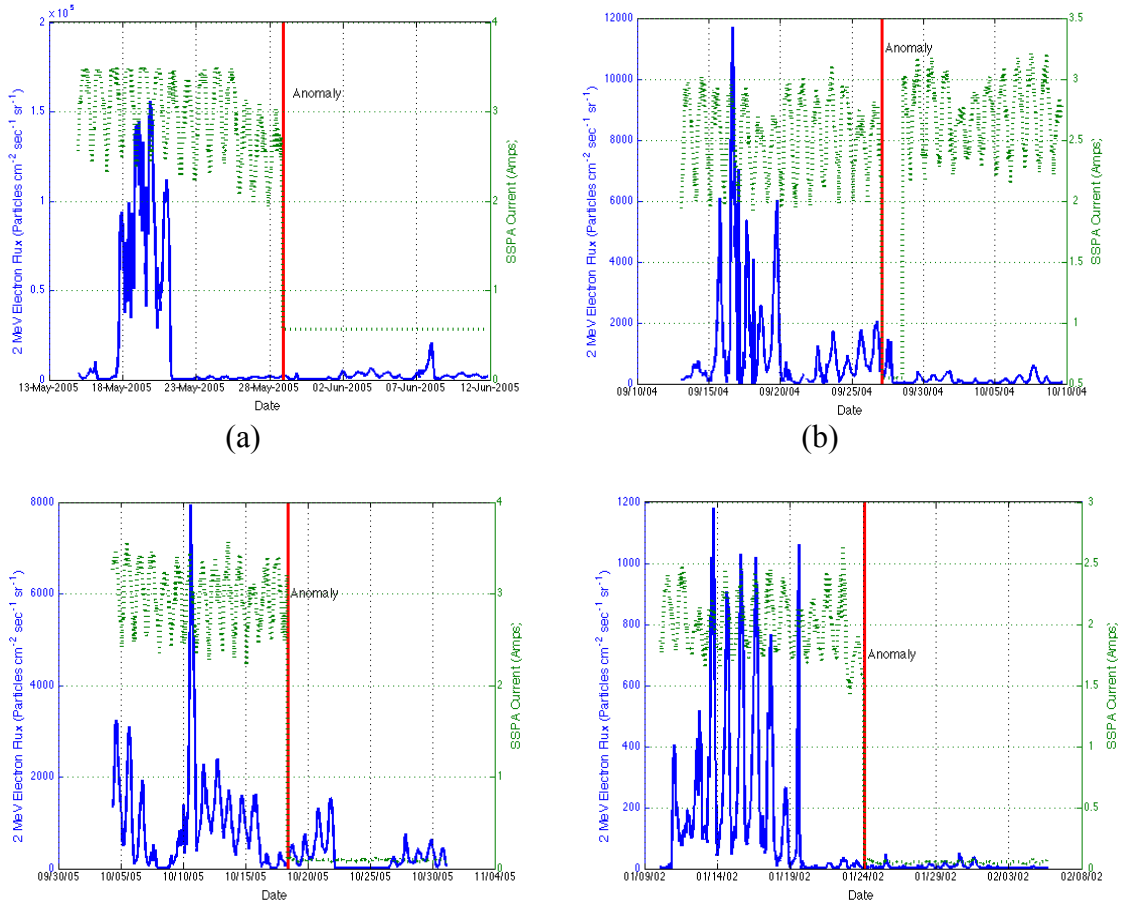

Figure 6(a-d). 2 MeV electron flux during SSPA anomaly for two weeks before and after four anomalies (a-d). GOES 2 MeV electron flux plotted on the left vertical axis, and SSPA current plotted on the right axis. The GOES 2 MeV electron flux is the blue line, the SSPA current is the dotted green line, and the anomaly is marked with a red line. The higher frequency variability in both electron flux and current is due to the diurnal cycle.

Figure 6 clearly shows that a drastic increase of 2 MeV electron flux occurs approximately one to two weeks before the selected anomalies and may alter the current carrying capabilities of the SSPA. The number of days between the peak 2 MeV electron flux and the four anomalies in Figure 6(a-d) is 10.6 days for 6(a), 10.4 days for 6(b), 7.8 days for 6(c), and 10.4 days for 6(d). We will analyze the other amplifier anomalies aboard the Telenor satellites to determine whether this observation is consistent amongst other satellites as well.

While most of the anomalies occurred during the part of the solar cycle when electron fluxes are enhanced, there did not appear to be an obvious relationship between the anomalies and 1.8-3.5 MeV electron fluxes at the time of anomaly. However, eleven of the twenty-six anomalies experienced elevated electron flux approximately one to two weeks prior to the anomaly. One potential explanation could be a combined effect or relativistic electrons and galactic cosmic rays. GCRs probability also increases as solar cycle declines. The analysis of our additional

satellite anomaly data will help clarify if some of the anomalies may be related to the increases in electron fluxes, and help understand the elevated flux phenomena one to two weeks prior to anomalous behavior.

2.4.1.4. SSPA Anomalies and High Energy Protons

In our previous analysis we investigated the 30 MeV proton flux for a period of five days before each anomaly and one day after [*Lohmeyer et al.,* 2012]. Since this analysis, we have extended our period of analysis to two weeks prior to each anomaly. Figure 7 shows the three SSPA anomaly scenarios that experienced atypical 30 MeV proton flux for a period of up to five days prior to the anomaly.

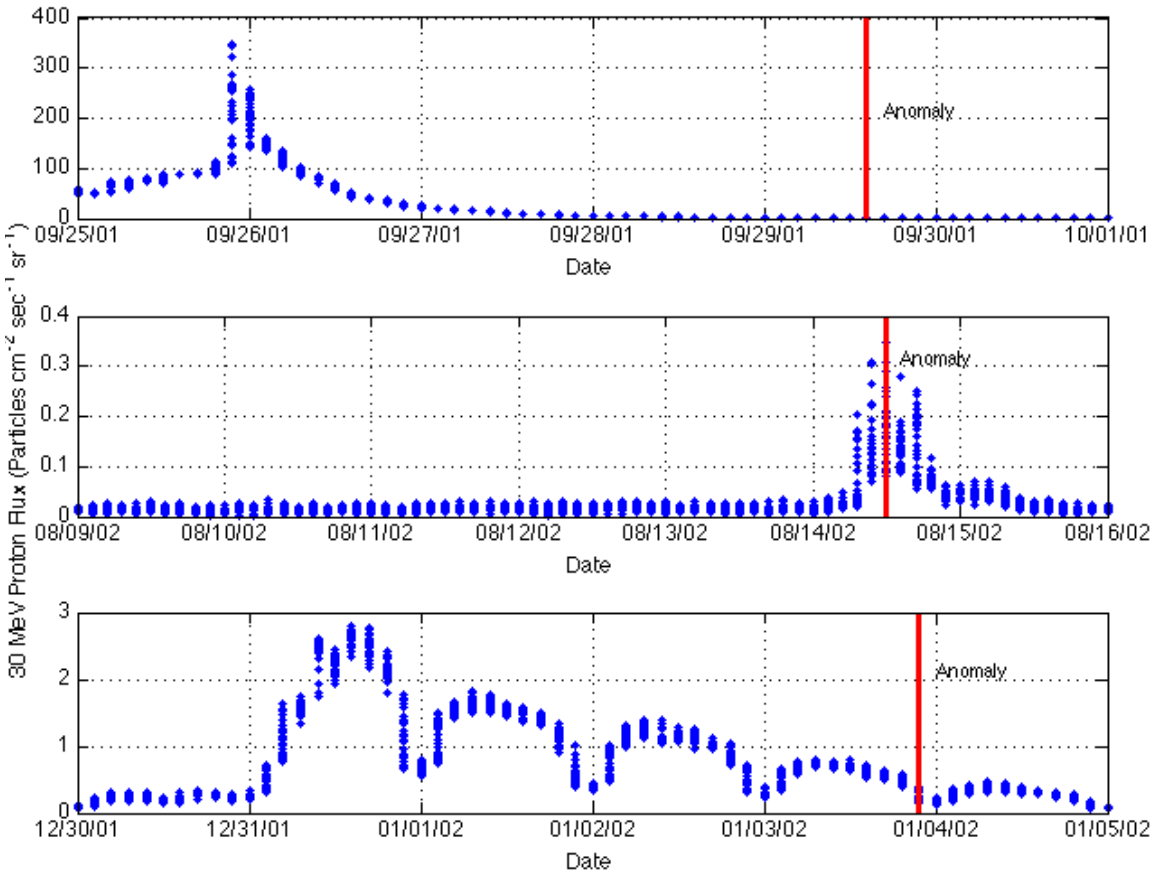

Figure 7. 30 MeV Proton Flux for a period of five days before and one day after three of the twenty-six SSPA anomalies [*Lohmeyer et al.,* 2012]

Figure 7 motivates an interesting question pertaining to the relationship of high-energy protons and amplifier anomalies that we would like to pursue. Are the increases in 30 MeV proton flux related to the anomaly, or were they coincidental? This question was not previously addressed in our work, but we will investigate the relationship between high-energy proton flux and the Inmarsat and Telenor amplifier anomalies.

We are particularly interested determining the effect of high-energy protons on the amplifier components and their effect on solar array degradation, as presented in Section 2.4.2: Solar

Array Degradation. However to investigate the relationship of high-energy protons with amplifier anomalies, we will follow a similar approach as with Kp and the high-energy electron flux data where we found the distribution of the respective space environment measurements over the time the satellites of interest (Inmarsat, Telenor, etc.) are in operation. Then we will determine the level of higher energy proton flux, 10 MeV and 30 MeV, at the time of the anomalies and up to two weeks prior to the anomalies to determine if a correlation exists between high-energy protons and amplifier anomalies, as well as high-energy protons and solar array degradation. This approach is taken in numerous studies of the same nature and is described in *Violet et al.* [1993].

2.4.1.5. SSPA Anomalies and Galactic Cosmic Rays

We have not yet analyzed SSPA anomalies in comparison with galactic cosmic ray flux. However, we are in the process of obtaining GCR flux data and will take the same approach in understanding the relationship of the anomalies with GCRs as we conducted with the preceding particle populations. We will understand the GCR flux over the entire operating flux of the satellites by finding the mean and standard deviation of GCR flux distribution between 1996-2012. Then we will determine the flux level at the time of the anomaly, as well as up to two weeks prior to the anomaly in order to better understand the space environment prior to the event. Once we can quantify the flux levels for this period of time prior to the anomalies of the Inmarsat and Telenor satellites, we can determine whether GCRs are indeed a contributor to these satellite component failures.

2.4.1.6. The Local Time of the SSPA Anomalies

Numerous studies, e.g. *Wilkinson* [1994], *Fennel et al.* [2001], *Iucci et al.,* [2006], *Choi et al.* [2011], suggest that satellite anomalies from surface charging effects depend on satellite local time, as surface charging anomalies generally tend to occur between midnight and dawn. Internal charging often occurs at times near local noon, but can also occur outside of this time sector [*Fennel et al.,* 2001; *Wrenn et al.,* 2002]. Choi *et al.* [2011] found that for 95 GEO anomalies 72% of the anomalies occur between midnight to and dawn in local time. In *Choi et al.* [2011] the anomalies are not only SSPAs but also include a variety of additional failures.

In Figure 8, we plot the local time of each of the 26 SSPA anomalies on the eight Inmarsat satellites. Fleet A is represented with red circles, and Fleet B is shown in black asterisks. The radial distance from the center of the graph has no significance, but is used for clarity, since several anomalies occur at similar local times. In the future we will conduct this analysis for the other satellite in our study to determine the local time distributions of those fleets, and if any similarities across fleets occur.

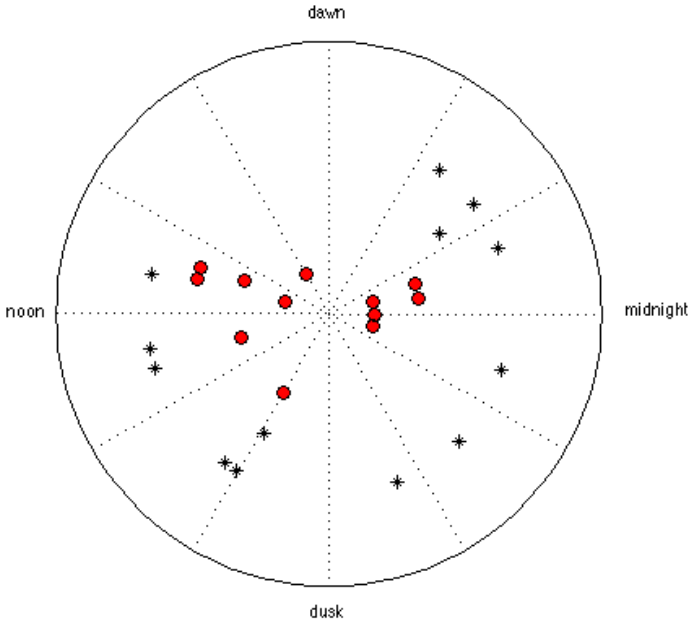

Figure 8. Local time for the twenty-six SSPA anomalies onboard Fleet A (red circles) and Fleet B (black asterisk). The radial distance from the center of the plot is an offset for clarity and has no other significance.

The 26 SSPA anomalies may not be sufficient to draw clear conclusions on time dependence, although they are all from the same type of component failure. However, we will summarize their distribution, and expand upon this analysis in our future work. Of the thirteen SSPA anomalies in Fleet A, six (46%) occurred around local midnight, and the remaining seven (54%) occurred more loosely around local noon (one each closer to the dawn and dusk sectors than to local noon). For Fleet B, five of the thirteen occur in the approximately midnight to dawn sector (38.5%), and six (46%) occur in the local noon to dusk sector. The distribution cannot completely rule out surface charging for all of the anomalies but also does not appear to confirm the LT bias often seen in association with surface charging, which, as previously stated, primarily occurs in the dawn to local midnight period. We will conduct local time distribution analysis of the Telenor satellite anomalies to determine if

2.4.1.7 SSPA Anomalies and Eclipse Data

Satellites in GEO typically have a direct view of the Sun and thus are able to utilize energy from solar panels as a primary power source. However, in the event of an eclipse, the Earth blocks sunlight from reaching the solar arrays and requires satellite operators to monitor and control power use. The two eclipse seasons are late February to mid-April (Spring Eclipse Season) and late August to late October (Fall Eclipse Season). The longest eclipses generally last between 68 to 73 minutes [*Lohmeyer et al.*, 2012]. The eclipse seasons coincide with the vernal and autumnal equinox, because it is during equinox that the Earth blocks the Sun's light from reaching the satellites.

Choi et al. [2011] found that more of the geostationary satellite anomalies occurred in the spring (March, April, and May) and the fall (September, October, and November) than in the summer in winter. Spring and fall are known as periods when geomagnetic activity is at a maximum

[*Russell and McPherron*, 1973]. However, despite there being an observed semiannual variation in geomagnetic activity as well as in GEO anomalies [*Wilkinson,* 1994; *Iucci et al,* 2006], this result was not observed for the twenty-six SSPA anomalies on board the Inmarsat satellites. Table 4 shows the season in which each of the twenty-six SSPA anomalies occur. The specific satellite longitudes are kept anonymous to respect proprietary information.

Table 4. The number of SSPA anomalies per season on each of the Inmarsat satellites. Only seven of the satellites are tabulated, as one satellite did not experience any SSPA anomalies.

Satellite	Winter	Spring	Summer	Fall
A	1	1	0	0
B	1	3	0	4
C	0	0	1	0
D	2	0	0	0
E	2	1	1	1
F	1	2	1	2
G	1	0	0	1
Total	8	7	3	8

No obvious seasonal trend for the anomalies exists. Half of the anomalies occurred in winter and fall, and the fewest number of anomalies occurred in the summer. Interestingly, January was the month with the most anomalies, but is a time when geomagnetic activity is at a minimum [*Russell and McPherron*, 1973]. One possible explanation of these results is that the geometry of the Earth eclipsing the Sun, in addition to the measures taken by the operators during eclipse seasons for power management, seems to reduce the number of SSPA anomalies. Incorporating the additional anomaly data will help determine if these types of components are susceptible to the previously noted seasonal dependencies of geostationary anomalies [*Iucci et al.,* 2006; *Wilkinson,* 1994; *Choi et al.*, 2011].

2.4.2. Solar Array Degradation

Very few studies have publicly presented analysis comparing the actual correlation of solar array telemetry to energetic particle flux or solar proton events. However, there is significant interest amongst both the satellite operator and space weather community to better understand the relationship between the space environment and solar array degradation. To quantify the effects of high-energy protons and galactic cosmic rays on solar arrays, we will analyze the solar array telemetry (open circuit voltage, and short circuit current across a single cell of outboard panel) to determine if the solar array degradation is gradual or if there are any periods of instantaneous degradation in the performance of the solar array. We will then identify these periods of time and statistically compare the telemetry with the flux data of high-energy protons (10 MeV and 30 MeV) and GCRs. We will also obtain dates of solar proton events to statistically compare with the solar array telemetry to determine if these events caused any clear degradation. This approach is consistent with our methodology presented in Section 2.4.1, which also follows the approach of numerous studies of similar nature, and is presented in *Violet et al.* [1993].

2.5 Anomalous Component Detection Algorithm

As noted in Section 2.2: Acquiring Geostationary Communication Satellite Data, the complete telemetry data archives are a "treasure trove" of combined science and engineering information on commercial communication components' response to space weather, and contain valuable information about how space weather impacts flight electronics and materials as a function of age, time, and location. The work in Section 2.4 investigates satellite systems at the time of recorded anomalies and compares the telemetry of these satellite systems with known space weather phenomenon. The main objective behind the analysis in this chapter is to statistically examine the telemetry over all time and determine if information pertaining to the satellite systems (e.g. satellite repositioning or component anomaly) or the space environment (e.g. elevated particle flux or major storm) can be gathered, and not just at periods of known anomalies. The specific data we will initially incorporate in this analysis are the amplifier currents and temperatures, solar array currents, and the total bus power. A major challenge with the usability of this algorithm is to design a way to input the telemetry that is uniform regardless of the format of the satellite operator, or that can efficiently handle different telemetry formats. This is particularly difficult, because the gathered data in its original state is of a variety of formats including different file types (Excel files, text files, etc.) and structures (column headers, telemetry units, etc.).

We will start by plotting the data over time to determine if obvious trends or anomalous behavior can be spotted by eye before designing search and characterization algorithms. One example of clear anomalous SSPA behavior is shown in Figure 9. From this we can create a preliminary definition for nominal or normal satellite behavior. This definition will enable us to detect anomalous performance.

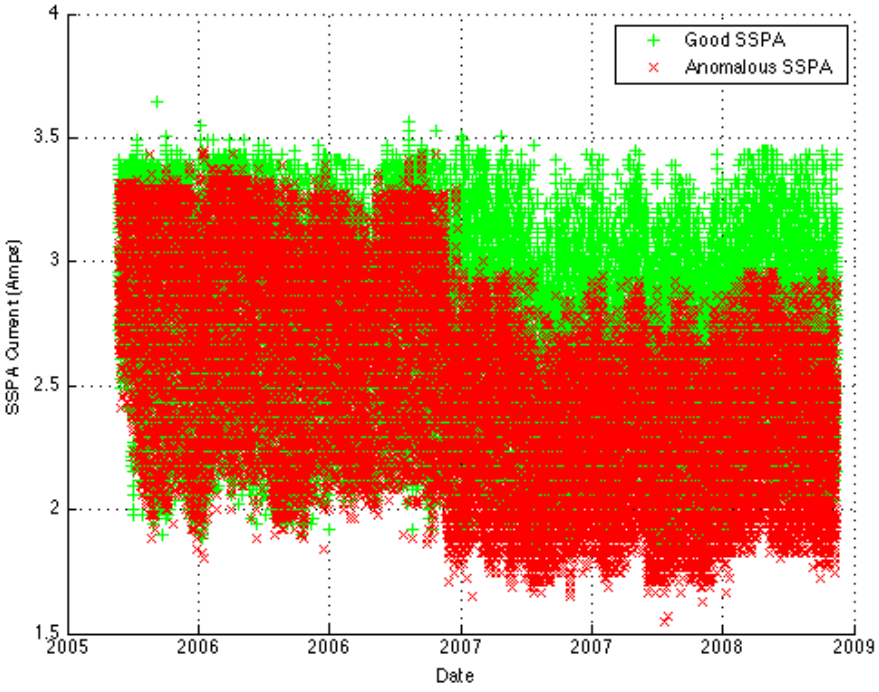

Figure 9. Obvious Anomalous SSPA Operation

Once we have identified anomalous areas by eye, we will write a MATLAB algorithm that inspects the telemetry and detects trends that aren't as obvious. We will incorporate the operator thresholds in our algorithm as a basic identifier of anomalous activity, as well as more sophisticated methods that can detect when anomalous behavior is occurring regardless of whether the satellite is operating inside the operator specified thresholds. One technique will be to compare telemetry to our normal operation definition and construct a distribution of how far from normal performance the component is operating and at what point in time the divergence from normal operation behavior began. Another technique is to take the derivative of the telemetry data and determine when a change in slope of the telemetry occurs. *Gubby et al.* [2002] found that anomalies particularly occur at sign reversals of 2 MeV electron flux. While this is an environmental parameter, and not one of the telemetry inputs of the algorithm, we are interested to determine if a similar situation occurs with the telemetry data.

Figure 10 shows the SSPA current averaged over three months between 1996-2012 for a good SSPA (shown in green) and an anomalous SSPA (shown in red). These two SSPAs are different than the ones shown in the previous figure. While both SSPAs experience a drastic decrease in SSPA current in 2005, the current values begin to diverge after this decrease. These current values are still within the operator threshold, but one of the SSPAs is recorded as experiencing an anomaly.

Figure 10. Three Month Averaged SSPA Currents

This figure also introduces another interesting question regarding the temporal resolution of the data. Often time telemetry is recorded with such high temporal resolution that data is gathered ever second or every five seconds. Processing the data at this increment can take a very large amount of time, and therefore binning the data into periods of hours or days is often incorporated in processing algorithms. Our algorithm will help identify over what time period to bin the

telemetry of this nature for anomaly detection and potentially anomaly prediction. Specific trends occur in a diurnal manner, therefore if one analyzes data by averaging over a period of one week they may miss important information that could help detect an anomaly.

We will also investigate the diurnal characteristics of the telemetry and write code to determine when changes in the telemetry over this period occur. Figure 11 clearly shows the diurnal cycle of the data. Each day the current experiences a minimum and maximum value.

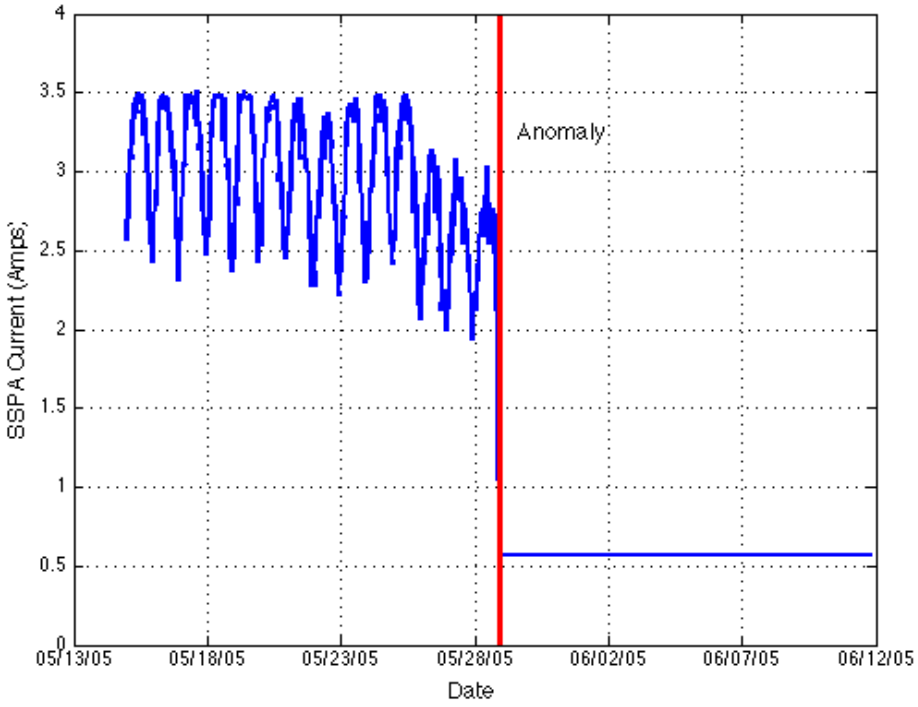

Figure 11. Diurnal Variation in SSPA Current Before Anomaly

For the maximum current measurements of the first five days are shown to be consistent at 3.5 Amps, followed by a slight decrease in the maximum daily current to approximately 3.37 Amps, followed by a significant decrease all the way to a maximum peak current of approximately 3.03 Amps, and then the SSPA anomaly occurs. The minimum daily current values are not as consistent as the daily peaks. In our algorithm we will incorporate a method for locating the daily peaks and daily minimum values and determining if and when these values are changing and to what extent they are changing.

Interestingly, at the time of the initial decrease in the daily peak current, a significantly elevated level of 2 MeV integral electron flux occurred, shown in Figure 6 of Chapter 3. We would also like to use or algorithm to investigate the increasingly popular statement amongst the satellite community that all satellites are space weather sensors. By incorporating our telemetry algorithm with known space weather occurrences we would like to answer, just how accurate are these satellites components at relaying information about the space environment?

We would also like to incorporate methods in our algorithm to understand if it is possible to identify causative agents for anomalous or atypical telemetry measurements. Was the deep drop

in current in 2005, shown in Figure 10, due to an orbital reposition? Was the satellite powered off? We would like to determine what information could be inferred from one piece of telemetry by categorizing known occurrences and telemetry behavior, and incorporating these types of performance levels in our algorithms.

2.6 Plan for Progression

Spring 2013

a. First committee meeting, Minor Approved
b. Defend Thesis Proposal
c. Obtain data from Telenor, and other satellite operators
d. Continue working on space weather and Inmarsat anomaly analysis – submit AGU Space Weather Paper, begin solar array degradation analysis

Summer 2013

a. Attend the NSF GEM Workshop and teach the "Geomagnetic Storms" lecture
b. Conduct extensive literature search on trends in communication satellite design
c. Continue analysis of space weather effects – finish up Inmarsat study, analysis of Telenor satellites, continue obtaining Echostar and other data
d. Begin TWTA vs. SSPA Analysis with Inmarsat and Telenor Fleets
e. Begin algorithm for anomalous satellite behavior

Fall 2013

e. Committee meeting.
f. Take statistics course and negotiation course (finish major and minor courses)
g. Write TWTA vs. SSPA analysis for part of the Trends in Modern Satellite Design section for Inmarsat and Telenor satellites, and reevaluate goals of study for items to complete
h. Finish Inmarsat space weather analysis, and continue/begin Telenor & Echostar analysis
i. Continue working on algorithm structure and implementation

Spring 2014

a. Committee meeting.
a. Begin dissertation – organize structure and assess goals and remaining "to dos"
b. Continue to work algorithm and analysis of satellites as space weather sensors
c. Continue to work on all satellite and space weather analysis – Attend 2014 Space Weather Workshop and present results of satellite anomalies

Summer 2014

a. Work on dissertation.
b. Attend IEEE NSREC – Nuclear and Space Radiation Effects Conference to present SSPA vs. TWTA Analysis, and solar array degradation analysis
c. Continue improving algorithm

Fall 2014

a. Committee meeting.
b. Work on dissertation, determine if any goals or questions are unanswered, and address those items.

Spring 2015

a. Committee meeting.
b. Finish dissertation
c. Defend.

References

Allen, J. (2010), The Galaxy 15 anomaly: Another satellite in the wrong place at a critical time, *Space Weather*, 8(6), S06008, doi: 10.1029/2010SW000588.

Aloisio, M., Angeletti, P., Colzi, E, D'Addio, S., Balague, R., Casini, E., Coromina, F. (2008), "End-to-End Performance Evaluation Methodology for TWTA-Based Satellite Flexible Payloads", IEEE International Vacuum Electronic Conference, 22-24 April 2008.

Aloisio, M., Angeletti, P., Coromina, F., Deborgies, F., Gaudenzi, R., Ginesi, A. (2010), "R&D Challenges for Broadband Satcomes in 2020", IEEE International Vacuum Electronics Conference, 18-20 May 2010.

Baker, D.N. (2000), The Occurrence of Operational Anomalies in Spacecraft and Their Relationship to Space Weather, *IEEE Transactions on Plasma Science,* 28(6), doi: 10.1109/27.902228.

Baker, D.N. (2002), How to Cope with Space Weather. *Science*. 297, doi: 10.1126/ science.1074956.

Barbieri, L.P. and R.E. Mahomot (2004), October-November 2003's space weather and operations lessons learned, *Space Weather*, 2, S09002, doi:20.2039/2004SW000064.

Bijeev, N.V., Malhotra, A., Kumar, V., Singh, S., Dasgupta, K.S., Motta, R.N., Venugopal, B., Sandhyarani, Jinan, O.K., and B.K. Jayakumar, (2011), "Design and Realization Challenges of Power Supplies for Space TWT" IEEE International Vacuum Electronic Conference, 21-24 Feb 2011.

Bodeau, M. (2010), High Energy Electron Climatology that Supports Deep Charging Risk in GEO, paper presented at 48th AIAA Aerospace Sciences Meeting Including the New Horizons Forum and Aerospace Exposition, Orlando, FL, 4-7 January 2010.

Choi, H.S., Lee, J., Cho, K.S., Kwak, Y.S., Cho, I.H., Park, Y.D., Kim, Y.H., Baker, D.N., Reeves, G.D., and D.K. Lee (2011), Analysis of GEO spacecraft anomalies: Space weather relationships, *Space Weather*, S06001, doi:10.1029/2010SW000597.

Cole, D.G. (2003), Space Weather: Its effects and predictability, *Space Science Reviews*, 107, 295-302, doi: 10.1007/978-94-007-1069-6_27.

Denton, M.H, Borovsky, J.E., Skoug, R.M, Thomsen, M.F., Lavraud, B., Henderson, M.G., McPherron, R.L., Zhang, J.C., Liemohn, M.W. (2006), Geomagnetic storms driven by ICME and CIR-dominated solar wind" *Journal of Geophysical Research* 111, doi:10.1029/2004JA011436.

Escalera, N., Boger, W., Denisuk, P., & Dobosz, J. (2000), Ka-band, 30 watts solid state power amplifier. In *Microwave Symposium Digest. 2000 IEEE MTT-S International* (Vol. 1, pp. 561-563). IEEE.

Feicht, J.R., Loi, K.N., Menninger, W.L., Nicolello, J.G., Zhai, X. (2012), "Space Qualified 140 W Linearized L-band Helix TWTA" IEEE International Vacuum Electronics Conference, 24-26 April 2012.

Fennel, J.F., H.C. Koons, J.L. Roeder, and J.B. Blake (2001), Spacecraft charging: Observations and relationships to satellite anomalies, *Aerosp. Rep. TR-2001(8570)-5,* Aerosp. Corp., Los Angeles, California.

GOES I-M Databook. Palo Alto, CA: Space Systems/Loral, 1996.

Gubby, R. and J. Evans (2002), Space environment effects and satellite design, *Journal fo Atmospehric and Solar-Terrestrial Physics*, 64, 1723-1733.

Hastings, D., and H. Garret (1996), *Spacecraft-Environment Interactions*, Cambridge University Press, New York, NY.

Horne, R.B, Glauert, S.A., Meredith, N.P., Boscher, D., Maget, V., Heynderickx, D., and Pitchford, D. (2013), Space weather impacts on satellite and forecasting 1 the earth's electron radiation belts with 2 SPACECAST, *Space Weather*, doi:10.1002/swe.20023.

Illokken, E. (1987). TWT Reliability in Space. *Aerospace and Electronic Systems Magazine, IEEE*, *2*(7), 22-24.

Iucci, N., Dorman, L.I., Levitin, A.E., Bevlov, E.A, Eroshenko, N.G., Villoresi, G., Chizhenkov, G.V., Gromova, L.I., Parisis, M., Tyasto, M.I., Yanke, V.G. (2006), Spacecraft operational anomalies and space weather impact hazards, *Advances in Space Research*, 37, 184-190, doi:10.1016/j.asr.2005.03.028.

Kaliski, M., (2009), "Evaluation of the Next Steps in Satellite High Power Amplifier Technology: Flexible TWTAs and GaN SSPAs", IEEE International Vacuum Electronics Conference, 28-30 April 2009.

Kamide, Y., Baumjohann, W., Daglis, I.A., Gonzalez, W.D., Grande, M., Joselyn, J.S., McPherron, R.L., Phillips, J.L., Reeves, E.G.D, Rostoker, G., Sharma, A.S., Singer, H.J., Tsurutani, B.T., Vasyliunas, V.M. (1998), Current understanding of magnetic storms: Storm-substorm relationships, *Journal of Geophysical Research*, 103(A8), 17705-17728, doi: 10.1029/98JA01426.

King, J.H. and N.E. Papitashvili (2004), Solar wind spatial scales in and comparisons of hourly Wind and ACE plasma and magnetic field data, J. Geophys. Res., Vol. 110, No. A2, A02209, 10.1029/2004JA010804.

Koons, H.C., Mazur, J.E., Selesnick, R.S., Blake, J.B., Fennel, J.F., Roeder, J.L. and P.C. Anderson (2000), The Impacts of the Space Environment on Space Systems, 6th Spacecraft

Charging Technology Conference, Air Force Research Laboratory Science Center, Hanscom Air Force Base, MA.

Lanzerotti, L.J., C. Breglia, D.W. Maurer, G.K. Johnson III, and C.G. Maclennan (1998), Studies of spacecraft charging on geosynchronous telecommunications satellite, *Adv. Space Res.,* 22, doi:10.1016/SO273-1177(97)01104-6.

Lai, S. (2012), *Fundamentals of Spacecraft Charging,* Princeton University Press, Princeton, New Jersey.

Li, X., Baker, D.N., Temerin, M., Reeves, G., Friedel, R., and Shen, C. (2005), Energetic Electrons, 50 keV to 6 MeV at geosynchronous orbit: Their responses to solar wind variations, *Space Weather*, 3, S04001, doi: 10.1029/2004SW000105.

Lohmeyer, W., K. Cahoy, and D.N. Baker (2012), Correlation of GEO Communication Satellite Anomalies and Space Weather Phenomena: Improved Satellite Performance and Risk Mitigation, paper presented at 30th AIAA International Communications Satellite Systems Conference (ICSSC), Ottawa, Canada.

Lohmeyer, W., K. Cahoy, and S. Liu (2013), Causal relationships between solar proton events and single event upsets for communication satellites, paper presented at the 2013 IEEE Aerospace Conference, Big Sky, Mont., March 2-9.

Love, D.P., D.S. Toomb, D.C. Wilkinson, and J.B. Parkinson (2000), Penetrating electron fluctuations associated with GEO spacecraft anomalies, *IEEE Trans. Plasma Sci.,* 28, doi:10.1109/27.902234.

Mallon, K.P., (2008), "PL.6: TWTAs for Satellite Communications: Past, Present, and Future", IEEE, p. 14-15.

Mazur, J.E. and T.P. O'Brien (2012), "Comment on "Analysis of GEO spacecraft anomalies: Space weather relationships" by Ho-Sung Choi et al." *Space Weather*, 10, doi: 10.1029/2011SW000738.

Miyoshi, Y., and Kataoka, R. (2008), Flux Enhancement of the outer radiation belt electrons after the arrival of stream interaction regions, *Journal of Geophysical Research*, 113, A03S09, doi:10.1029/2007JA012506.

Murthy, H.S., Sharma, A., Badarinarayana, K., and P. Lakshminarasimhan (2011), "Thermal Management of GEO Satellite Communication Payload" IEEE International Vacuum Electronics Conference, 21-24 April 2011.

National Weather Service. "NOAA / NWS Space Weather Prediction Center." *NOAA / NWS Space Weather Prediction Center*. National Oceanic and Atmospheric Administration, 5 Nov. 2007. Web. 23 Mar. 2012. http://www.swpc.noaa.gov/.

NRC (2008), "Severe Space Weather Events – Understanding Societal and Economic Impacts Workshop" *National Research Council*. National Academy of Sciences. http://www.nap.edu/catalog/12507.html.

O'Brien, T. P. (2009), SEAES-GEO: A spacecraft environmental anomalies expert system for geosynchronous orbit, *Space Weather,* 7(9), S09003, doi:10.1029/2009SW000473.

O'Brien, T.P., Mazur, J.E., and J.F. Fennel (2013), The priority mismatch between space science and satellite operations, *Space Weather*, 11(2), doi: 10.1002/swe.20028.

Rapisarda, M., Colzi, E., Angeletti, P., Aloisio, M., (2010), "Navigation Traveling Wave Tube Amplifiers – Trade-off Aspects" IEEE International Vacuum Electronics Conference, 18-20 May 2010.

Reeves, G.D., McAdams, K.L., Friedel, R.H.W. (2003), Acceleration and loss of relativistic electrons during geomagnetic storms, *Geophysical Research Letters,* 30(10), 1529, doi:10.1029/2002GL016513.

Reeves, G. D., S. K. Morley, R. H. W. Friedel, M. G. Henderson, T. E. Cayton, G. Cunningham, J. B. Blake, R. A. Christensen, and D. Thomsen (2011), On the relationship between relativistic electron flux and solar wind velocity: Paulikas and Blake revisited, J. Geophys. Res., 116, A02213, doi:10.1029/2010JA015735.

Riley, Pete (2012), On the probability of occurrence of extreme space weather events, AGU Space Weather, Vol. 10, SO2012, doi: 10.1029/2011SW000734.

Robbins, N. R., Christensen, J. A., & Hallsten, U. R. (2005), Performance and reliability advances in TWTA high power amplifiers for communications satellites. In *Military Communications Conference, 2005. MILCOM 2005,* 1887-1890.

Robbins, N., Dibb, D., Menninger, W., Zhai, X., Lewis, D. (2012), "Space Qualified, 75-Watt V-band Helix TWTA", International Vacuum Electronics Conference, 24-26 April 2012.

Royal Observatory of Belgium. SIDC - Solar Influences Data Analysis Center. *SIDC - Solar Influences Data Analysis Center.* 28 Aug. 2003. Web. 25 June 2012. <http://sidc.oma.be/sunspot-data/>.

Russell, C.T., and McPherron, R.L. (1973), Semiannual Variation of Geomagnetic Activity, *Journal of Geophysical Research,* 78(1), 92-108, doi: 10.1029/JA078i001p00092.

Schulz, M., and Lanzerotti, L. J. (1974), *Particle diffusion in the radiation belts*, Springer-Verlag, N.Y.

Schwank, J.R., Shaneyfelt, M.R., and P.E. Dodd (2008), Radiation Hardness Assurance Testing of Microelectronic Devices and Integrated Circuits: Radiation Environments, Physical

Mechanisms, and Foundations for Hardness Assurance, *Sandia National Laboratories Document,* SAND-2008-6851P.

Sechi, Franco, and M. Bujatti (2009), *Solid-state Microwave High-power Amplifiers*. Artech House, M.A.

Shea, M.A. and Smart, D.F. (1998), Space Weather: The Effects on Operations In Space *Adv. Space Res.* 22(1), 29-38, doi: 10.1016/S0273-1177(97)01097-1.

Strauss, R. (1993), Orbital Performance of Communication Satellite Microwave Power Amplifiers (MPAs), *International Journal of Satellite Communications,* 11, 279-285.

Strauss, R. (1994), Reliability of SSPA's and TWTA's, *IEEE Transactions on Electron Devices* 41(4), 625-626.

Thomsen, M.F. (2004), Why Kp is such a good measure of megnetospheric convection, *Space Weather*, 2(11), doi: 10.1029/2004SW000089.

Tretkoff, E. (2010), Space Weather and Satellite Engineering: An Interview with Michael Bodeau, *Space Weather,* 8, SO3003, doi:10.1029/2010SW000584.

Tsurutani, B., Gonzalez, W.D., Gonzalez, A.L.C., Tang, F., Arballo, J.K., and Okada, M. (1995) Interplanetary origin of geomagnetic activity in the declining phase of the solar cycle, *J. Geophys. Res.,* 100, 21717.

Wilkinson, D.C., Daugtridge, S.C., Stone, J.L., Sauer, H.H., and P. Darling (1991), TDRS-1 Single Event Upsets and the Effect of the Space Environment, *IEEE Transactions on Nuclear Science*, 38(6).

Wilkinson, D.C. (1994), National Oceanic and Atmospheric Administration's spacecraft anomaly data base and examples of solar activity affecting spacecraft, *J. Spacecr. Rockets, 31*, doi:10.2514/3.26417.

Wilkinson, D.C., Shea, M.A., Smart, D.F. (2000), A Case History of Solar and Galactic Space Weather Effects on the Geosynchronous Communications Satellite TDRS-1, *Adv. Space Res.*, 26(1), 27-30.

Weekley, J.M, and Mangus, B.J. (2005), TWTA Versus SSPA: A Comparison of On-Orbit Reliability Data, *IEEE Transactions on Electron Devices,* 52(5), 650-652.